MEASURING THE QUALITY OF GENERALIZED GRADIENT APPROXIMATIONS IN A DENSITY FUNCTIONAL THEORY PSEUDOPOTENTIAL ENVIRONMENT FOR SOLIDS

A THESIS

SUBMITTED TO THE GRADUATE SCHOOL

IN PARTIAL FULFILLMENT OF THE REQUIREMENTS

FOR THE DEGREE

MASTER OF SCIENCE

BY

ZACHARY NAULT

DR. ANTONIO CANCIO

BALL STATE UNIVERSITY

MUNCIE, INDIANA

MAY 2014

Contents

List of Figures

List of Tables

Acknowledgements

First and foremost, I need to thank Dr. Cancio for the continual guidance through this epic quest of completing this thesis. It has been a long journey though treacherous swamps of misplaced knowledge and forgotten words. Without his teaching and reminding I am sure that half of this thesis would have fallen out of my head long before it ever made it to the page. Thank you.

Thank you also to those that agreed to be on my thesis committee. What you hold is a beast of a thesis and I applaud you for taking it on. I recommend a large cup of coffee.

Final thanks to my wife Kristie for her constant support and badgering to make sure I got this thesis done, and also for her taking the time to listen to me vent about my life that was this thesis. With all my love, thank you.

Chapter 1

Introduction

1.1 Density Functional Theory

Over the past 20 years density functional theory (DFT) has become a popular tool in the areas of condensed matter, chemistry, nanoscience, and biophysics. It allows for accurate calculations of the ground-state energies for any electronic system by only needing to know the density of the electrons. This method was pioneered by P. Hohenberg and W. Kohn [1] where they showed the connection between external potentials, total energy and electron density. DFT was refined by W. Kohn and L. J. Sham [2] using an auxiliary system of non-interacting particles. Doing so simplified the energy calculation, leaving only a single unknown, the exchange-correlation (XC) energy. If this XC energy could be found, then all other information about the system would be obtainable. This simplification also had another affect; it turned a calculation based on a many-body Hamiltonian in terms of the single electrons to a single-body Hamiltonian in terms of the density. This greatly decreased the computation time allowing for its use in many complex systems. For example, One very complex system is a DNA strand; in 2001 a group at Oakland University studied

the proton transfer within DNA base pairs using DFT [3]. Another place where DFT is used involves carbon nanotubes such as studying the effects of structure on electron transport [4].

1.2 Exchange-Correlation Energy

The only unknown within DFT, and a large focus of research, is the XC energy. This energy contains the information on how the electrons interact with one another within a system because of the Pauli exclusion principle and Coulomb repulsion. As there has yet to be a universal form found for the XC energy, it needs to be approximated; the simplest attempt is the local density approximation (LDA) [2]. The LDA treats the energy of the electron density at a single point in space like the energy of a homogeneous electron gas (HEG) at the same density. Because the density is a function based on location and the LDA is based on the density, the LDA is known as a functional of the density. Improving upon the LDA, there are generalized gradient approximations (GGA) which include information about the gradient of the density at a point in space. Currently, there are over 300 different forms of GGA's available, each designed with different theoretical constraints, experimental fits, and intended uses [5]. This vastness of options shows that many use and need GGA's but no universal functional has yet to be derived. One of the most common functional used within DFT today is the PBE [6] named after the creators: Perdew-Burke-Ernzerhof. The PBE is a GGA built with theoretical constraints, no experimental fits, and intended for most elements and systems. It is because of it's abundant use, that it is a major focus of this research. One variant of PBE is designed to perform better for solids: PBEsol [7]. As this research focuses on solid systems this functional is also a target for testing. A fairly recent functional known as APBE [8] is another

variant of the PBE but designed for atomic systems. As it is new, APBE has little research done with solids; therefore, it was chosen to be the final target functional.

1.3 Pseudopotentials

Within DFT there are two primary forms of calculating the ground-state properties of the system: all-electron (AE) and pseudopotential (PsP). An AE-type calculation takes into account every electron within the system. This form of calculation provides the most accurate result but is the most computationally expensive. PsP's, on the other hand, remove the core electrons under the frozen-core approximation [9] leaving only the chemically active valence electrons to be dealt with explicitly. This is done under the condition that the pseudo-orbital must match the real orbital beyond a fixed radial cut-off value. This allows for faster calculations with a minimal loss in accuracy.

Even though AE calculations are by far the more accurate choice, the most commonly used method in solids is the PsP calculation. This presents an interesting situation regarding the XC functionals used. All functionals are tested within the AE environment because of its accuracy, but then are used within PsP environments.

1.4 The Thesis Work

There were three goals that this research set out to accomplish. The first was to answer the question whether or not PsP calculations still provide accurate results like those from an AE calculations. To determine if our results were accurate, we looked for two features: reproducing the trends in the data seen with AE results and the relative percent difference compared to AE results. When testing models

it is common to select solids from all types of systems including ionic compounds, semiconductors, simple metals, and transition metals. A set of solids from those systems were tested using GGA's but with PsP's instead of AE calculations. By calculating typical properties (lattice constant, bulk modulus and cohesive energy) and comparing them with the other theoretical calculations along with experiment, the PsP performance can be gauged.

The second goal was to gauge the effects of using a PsP describing the core electrons with one functional type and a different functional type to describe the valence. This type of issue arises due to the limited number of pre-made PsP's available via the web. As it is easier to use a PsP from an online library then generating one of your own, you become limited by the types offered. This means that you may mismatch the functional type between the core and valance electrons. By mixing a PsP of one functional with a DFT calculation of another, calculating the ground-state properties, and comparing them with other theories, the effect of the mismatch can be characterized.

The third goal was to characterize the differences between the different functionals used within this thesis. Once the performance of PsP calculations and the effect of mixing core and valence functional types, the real differences between the functionals can be observed. This will provide a benchmark as to how other functionals may perform within the PsP environment for future work.

1.5 A Preview

Chapter 2 covers the theoretical background and description of DFT. A focus is given to XC functionals along with the LDA and the GGA. The theory behind PsP's and how they fit into DFT is detailed. Lastly, a basic outline of the methodology of this

research is given.

Chapter 3 details the test set of 16 solids gathered for this research. It provides a description of the convergence parameters for each solid and single atoms. The target properties: lattice constant, bulk modulus, and cohesive energy, are also detailed along with the steps to calculate them.

Chapter 4 dives into the realm of PsP's. It describes PsP libraries and what PsP types are available along with their limits. It details the need to generate our own PsP's and what types of information is needed to do so. Then, chapter 4 touches on the codes that can generate custom PsP's and why we have chosen to use the coding package APE. The results of testing our custom PsP's with the libraries is detailed along with a consistent scheme used to generate PsP's within this research.

Chapter 5 will explore the main questions of this research regarding the performances of PsP's and GGA's. The first section address how well the PsP calculation matchs the AE results for the target ground-state properties. The second section will address how well our results match experiment and the effects of the different functionals. In addition, the effect of describing the core electrons with a different XC functional than the valence electrons will be explored.

Chapter 6 contains a discussion on the limits of PsP's first touched on in chapter 4. Also, the conclusions from chapter 5 will be discussed with a focus on answering the questions presented here.

For quick reference, appendix A has a list of all the acronyms used with in this thesis. It provides a short description of the acronym as well.

Chapter 2

Density Functional Theory

2.1 Basics of DFT

Picture in your mind a system of N non-relativistic electrons and a collection of arbitrarily placed nuclei. Now, if the ground-state energy of this system could be calculated then other properties such as bond energies and bond lengths or lattice structure and bulk modulus could be predicted. In reality both the electrons and the nuclei are moving about the system making this difficult to keep track of. This can be solved if we assume that the nuclei are stationary compared to the electrons. This is know as the Born-Oppenheimer [10] approximation and allows the system to be interpreted as electrons moving in a constant positive potential. The Hamiltonian of this system would then look like

$$\hat{H} = \hat{T} + \hat{V}_{ee} + \hat{V}_{ext} \tag{2.1}$$

where the kinetic energy is

$$\hat{T} = -\frac{1}{2}\sum_{j=1}^{N} \nabla_j^2 \tag{2.2}$$

the electron-electron Coulomb repulsion is

$$\hat{V}_{ee} = \frac{1}{2} \sum_{i \neq j} \frac{1}{|\mathbf{r}_i - \mathbf{r}_j|} \tag{2.3}$$

and the external potential, electrons' interactions with the nuclei, is

$$\hat{V}_{ext} = -\sum_{j} \sum_{a} \frac{Z_a}{|\mathbf{r}_j - \mathbf{R}_a|} \tag{2.4}$$

with $\mathbf{r}_i, \mathbf{r}_j$ denoting electron positions, $\mathbf{R}_a$ a nuclei position, and Z_a the atomic number of the nuclei. It should be noted that this work uses atomic units setting $e^2 = \hbar = m_e = 1$ so energies are in Hartree (1 Ha = 27.2eV) and distances are in Bohr radii (1 bohr = 0.529 $\mathring{A}$). Equation (2.1) can then be solved for any electronic system providing the eigenenergies and all information about the system. However, this is no small task as this is an N body problem which increases in difficulty as the system grows in size and complexity. The problem of finding the exact solution can be passed off to computers but requires sophisticated calculations that take large amounts of computer time. Thus, there is a need to solve this ground-state problem of electronic systems with reasonable accuracy without a computational cost that becomes too prohibitive as the systems become larger. This is where density functional theory (DFT) enters the scene.

Starting from the Hohenberg-Kohn theorems [1] we can start to convert the Hamiltonian into a single body problem, which is far easier to solve. The first theory is: for any system of interacting particles the external potential, V_{ext}, can be uniquely determined from the ground-state density of the system. Normally, the wavefunction of a system is dependent on the kind of external potential within the system. As the potential will be the only change from one system of electrons to another, it can be connected to the ground-state density.

The second theory of Hohenberg and Kohn states that there is a universal functional of the ground-state energy, $E[n]$, in terms of the ground-state density.

$$E[n] =< \Psi_0[n]|\hat{T} + \hat{V}_{ee} + \hat{V}_{ext}|\Psi_0[n] > \tag{2.5}$$

Here, $\Psi_0[n]$ is the ground-state wavefunction in terms of the ground-state density, n. Then, the total energy of the system becomes defined by the density

$$E[n] = T[n] + E_{ee}[n] + E_{ext}[n] \tag{2.6}$$

This is a powerful statement; one only needs to know the functional $E[n]$, the correct E_{ext} for the system, and with the variational principle find an n that minimizes it. This provides an upper bound to the ground-state energy and all information of the system is found without a single wavefunction.

Even though this bridge between energy and density now exists, finding the unknowns within equation (2.6) is no easy task. Kohn and Sham [2] addressed this problem by solving an auxiliary system of non-interacting electrons that produces a non-interacting density which is equal to the ground-state density. The Hamiltonian for this system then looks like

$$\hat{H}_{aux} = -\frac{1}{2}\nabla^2 + \hat{V}^{\sigma}_{eff} \tag{2.7}$$

where the first term is the kinetic energy and the second is an effective local potential that affects an electron in space $\mathbf{r}$ with spin σ. The density of this system can be expressed as a sum over the electron probabilities at a point $\mathbf{r}$

$$n(\mathbf{r}) = \sum_{\sigma}\sum_{i}^{N^{\sigma}} |\Psi^{\sigma}_i(\mathbf{r})|^2 \tag{2.8}$$

Kohn-Sham (KS) then wrote the energy of this system in the form

$$E_{KS}[n] = T_{KS}[n] + \int V_{ext}(\mathbf{r})n(\mathbf{r})dr + E_H[n] + E_{II} + E_{XC}[n] \tag{2.9}$$

Here, $T_{KS}[n]$ is the kinetic energy of the orbitals, V_{ext} is the external potential caused by electron-ion interaction, E_{II} is the ion-ion energy (which by definition does not effect the electrons), $E_H[n]$ is the Hartree energy in the form

$$E_H[n] = \frac{1}{2}\int\int \frac{n(\mathbf{r})n(\mathbf{r}')}{|\mathbf{r}-\mathbf{r}'|}d^3r \tag{2.10}$$

the static charge density energy, and $E_{XC}[n]$ is the exchange-correlation(XC) energy. The XC energy has been chosen to satisfy the condition that this non-interacting system will produce the true ground-state energy, $E[n]$. Unfortunately this means the E_{XC} is an unknown that will need to be solved for. This energy will be addressed in section 2.1.1.

Now, working backwards from equation (2.9) the Hamiltonian of the system can be derived. Doing so, will allow for a comparison between this new Hamiltonian and that mentioned in equation (2.7), revealing information about V^{σ}_{eff}. This is accomplished by minimizing the KS energy with respect to the orbitals, subject to the constraint that the orbitals are non-zero

$$\frac{\delta E_{KS}}{\delta \Psi_i^{\sigma *}(\mathbf{r})} = \frac{\delta T_{KS}}{\delta \Psi_i^{\sigma *}(\mathbf{r})} + \left[\frac{\delta E_{ext}}{\delta n(\mathbf{r},\sigma)} + \frac{\delta E_H}{\delta n(\mathbf{r},\sigma)} + \frac{\delta E_{XC}}{\delta n(\mathbf{r},\sigma)}\right]\frac{\delta n(\mathbf{r},\sigma)}{\delta \Psi_i^{\sigma *}(\mathbf{r})} = \epsilon_i \Psi_i^{\sigma}(\mathbf{r}) \tag{2.11}$$

The eigenvalue comes from the Lagrange multipliers used to impose the constraint [11]. The the first term just becomes the kinetic energy term of the Hamiltonian

$$\frac{\delta T_{KS}}{\delta \Psi_i^{\sigma *}(\mathbf{r})} = -\frac{1}{2}\nabla^2 \Psi_i^{\sigma}(\mathbf{r}) \tag{2.12}$$

and the orbital derivative of the density is

$$\frac{\delta n(\mathbf{r},\sigma)}{\delta \Psi_i^{\sigma *}(\mathbf{r})} = \Psi_i^{\sigma}(\mathbf{r}) \tag{2.13}$$

Using this information with Lagrange multipliers, we can construct a KS type Hamiltonian:

$$(\hat{H}^{\sigma}_{KS} - \epsilon_i^{\sigma})\Psi_i^{\sigma}(\mathbf{r}) = 0 \tag{2.14}$$

Knowing that the wavefuction can not equal zero, the terms in the parentheses must be zero. Also, the Lagrange multipliers are the energies for the Hamiltonian; therefore, we can use equation (2.11) for the $\epsilon_i^\sigma \Psi_i^\sigma(\mathbf{r})$ term.This produces the full KS Hamiltonian

$$\hat{H}_{KS} = -\frac{1}{2}\nabla^2 + V_{KS}^\sigma \tag{2.15}$$

where V_{KS}^σ is the terms in brackets from equation (2.11). Since the only unknown is the XC energy, we have a definition for our XC potential

$$V_{XC}^\sigma = \frac{\delta E_{XC}}{\delta n(\mathbf{r}, \sigma)} \tag{2.16}$$

This completes the bridge between energy and density, now with only one unknown. However, it is important to note with this method one starts with a density and ends with a density. In order to make sure the calculation was done correctly the starting and ending densities should equal. This forces calculations to be self-consistent.

2.1.1 Exchange-Correlation Energy

Mentioned in the the previous section, the XC energy is an additional term so that the energy of the non-interacting system will provide the true ground-state energy. That means we can link equation (2.6) and (2.15) by setting $E_{KS}[n] = E[n]$. Then the unknown, $E_{XC}[n]$ can be solved for

$$E_{XC}[n] = (T[n] - T_{KS}[n]) + (E_{ee}[n] - E_H[n]) \tag{2.17}$$

Conveniently, the energy from the external potential in the KS approximation is that of the real system and all dependence on the external potential drops away. This provides a clue as to what the XC energy represents within the system; the difference in kinetic and internal interaction energies of the real system from the auxiliary system. This makes sense as the auxiliary system lacks any information on electron

interactions so it must be encapsulated within the XC energy. We can also see that XC energy is two separate types of interaction energies folded into one: E_X and E_C

$$E_{XC}[n] = E_X[n] + E_C[n] \tag{2.18}$$

The exchange energy, E_X is caused by Pauli statistics. Two electrons of the same spin are not allowed to occupy the same location in space, yet those of opposite spin are. Because of this, there is a change in the electrostatic energy associated with two particles in the same particular spin state. This is what factors into the exchange energy.

The correlation energy, E_C is connected to dynamic electron motions caused Coulomb interactions. Within a system the electrons will correlate with one another in order to reduce their interaction energies as low as possible. This is accomplished by electrons creating correlation holes, a region centred on the electron that acts like a positive charge. This means as electrons move away from one another in the system there is a point when they will no longer feel the electrostatic effects of the others.

If the true functional $E_{XC}[n]$ could be determined then the exact ground-state energy could be known for any many-body system by solving the single-body KS equations. However, the true form has yet to be found and $E_{XC}[n]$ has to be approximated. The following two sections detail methods for this approximation.

2.1.2 Local Density Approximation

The local density approximation (LDA) is built upon the idea of a system with slow varying electron density. This can be thought of in two different ways: slowly varying over a long length scale or changing rapidly with minimal amplitude compared to the average density (Figure 2.1). Under this assumption the density at any point in space can be treated like a homogeneous electron gas (HEG). A HEG is a system of

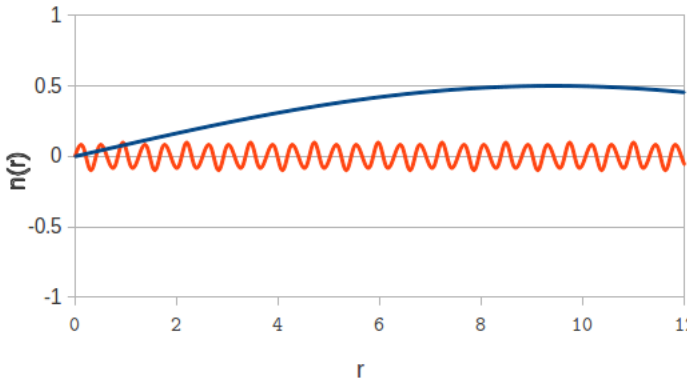

Figure 2.1: The two ways of viewing a system with a slow varying density. The first is slow changes over a long length scale. The second is rapid changes with small amplitudes compared to the average density.

interacting electrons at a uniform density within a positive charged background to maintain a neutral system. The main advantage of using the HEG to describe the system is that the exchange energy is known analytically. The exchange energy per particle at density n of the HEG is written as

$$\epsilon_x^{HEG}(r_s) = -\frac{3}{4\pi}\left(\frac{9\pi}{4}\right)^{\frac{1}{3}}\frac{e^2}{r_s a_0} \tag{2.19}$$

where r_s is the Wigner-Seitz radius of the HEG system at the density n.

$$r_s = \left(\frac{3}{4\pi n}\right)^{\frac{1}{3}} \tag{2.20}$$

The Wigner-Seitz radius is the radius of a sphere with the same volume as the average volume per electron in a solid. Under this approximation the entire system would have the same density, which would defeat our efforts, so a more clever approach needs to be taken. If $n(\mathbf{r})$ could be found at $\mathbf{r}$ then the total exchange energy could be found by multiping it with equation (2.19) and integrating over all space

$$E_x[n] = \int \epsilon_x^{HEG}[n(\mathbf{r})]n(\mathbf{r})d^3r \ , \tag{2.21}$$

providing the total exchange energy for the LDA approximation.

The correlation energy, on the other hand, needs to be solved for using numerical methods. This has been done in a few ways, but the method used here is the Ceperley-Alder calculation [12, 13] and has the form

$$\epsilon_c^{HEG} = \begin{cases} 0.0311\ln(r_s) - 0.048 + 0.002 r_s \ln(r_s) - 0.0116 r_s & r_s < 1 \\ \frac{-0.1423}{1+1.0529\sqrt{r_s}+0.3334 r_s} & r_s > 1 \end{cases} \tag{2.22}$$

Input into the LDA model we get

$$E_c[n] = \int \epsilon_c^{HEG}[n(\mathbf{r})] n(\mathbf{r}) d^3r \tag{2.23}$$

2.1.3 Generalized Gradient Approximation

The main goal of the generalized gradient approximation (GGA) is to improve upon the LDA by including information about the inhomogeneity of a system. This is done by including the gradient of the local density of the system. The exchange energy of the GGA can be written as

$$\epsilon_x^{GGA} = F_x(s^2)\epsilon_x^{HEG} \tag{2.24}$$

where $F_x(s^2)$ is known as the exchange enhancement factor which modifies the LDA exchange energy and is dependent on s, given by

$$s = \frac{|\nabla n|}{2k_f n} \tag{2.25}$$

which is a measure of the inhomogeneity of the system. It represents how fast the density is changing with respect to the Fermi wave vector k_f of the HEG, $k_f = (3\pi^2 n)^{\frac{1}{3}}$.

Over the years there has been many different forms proposed for $F_x(s^2)$. One of the most commonly used is know as the Perdew-Burke-Ernzerhof (PBE) functional [6].

The PBE exchange enhancement factor can be expressed as

$$F_x^{PBE}(s) = 1 + \kappa - \left(\frac{\kappa}{1 + \frac{\mu s^2}{\kappa}} \right) \tag{2.26}$$

The κ that appears in equation (2.26) is determined to be 0.804 in order for the exchange to adhere to the Lieb-Oxford bound [14] which is

$$E_x[n] \geq -1.679 e^2 \int n^{\frac{4}{3}} d^3 r \tag{2.27}$$

At the moment, consider μ as a numerical factor that controls the strength of the gradient correction. A more formal relationship will be developed later.

The correlation energy of the PBE starts with that of the LDA (eq. 2.22) but adds in a gradient based term

$$E_c^{GGA}[n] = \int n[\epsilon_c^{HEG}(r_s, \zeta) + H(r_s, \zeta, t)] d^3 r \tag{2.28}$$

where $\zeta = (n_\uparrow - n_\downarrow)/n$ is the relative spin polarization and t is a dimensionless density gradient

$$t = \frac{|\nabla n|}{2 \phi k_s n} \tag{2.29}$$

where $\phi = [(1+\zeta)^{\frac{2}{3}} + (1-\zeta)^{\frac{2}{3}}]/2$ is a spin scaling factor and k_s is the Thomas-Fermi screening length $k_s = (4\pi e^2 n)/\epsilon_0$. The gradient contribution H is constructed under three requirements. First, in the slowly varying limit ($t \to 0$), H is represented by its second order gradient expansion. Second, in the rapidly varying limit ($t \to \infty$) correlation must vanish as the system is unable to respond to the fast change. Finally, under uniform scaling to high density H must scale to a constant to cancel the ϵ_C^{HEG} term. These conditions are then satisfied when H is in the form

$$H = \frac{e^2}{a_0} \gamma \phi^3 \ln \left\{ 1 + \frac{\beta}{\gamma} t^2 \left[\frac{1 + A t^2}{1 + A t^2 + A^2 t^4} \right] \right\} \tag{2.30}$$

where

$$A = \frac{\beta}{\gamma} \left[\exp \left\{ \frac{-\epsilon_c^{HEG} a_0}{\gamma \phi^3 e^2} \right\} - 1 \right]^{-1} \tag{2.31}$$

with $\gamma = (1 - \ln 2)/\pi^2 \sim 0.031091$. There is one more constraint; under the high density ($r_S \to 0$), slowly varying ($t \to 0$) limits the XC should return the LDA's response to the system. Equation (2.26) of the exchange would be

$$F_x^{PBE}(s) \sim 1 + \mu s^2 \quad as\ s \to 0 \tag{2.32}$$

H would be

$$H \to -\frac{e^2}{a_0}\beta\phi^3 t^2 \quad as\ t \to 0 \tag{2.33}$$

and the total XC energy per particle would look like

$$(1 + \mu s^2)\epsilon_x^{HEG} + \epsilon_c^{HEG} - \frac{e^2}{a_0}\beta\psi^3 t^2 = [\epsilon_x^{HEG} + \epsilon_c^{HEG}] + [\mu s^2 \epsilon_x^{HEG} - \frac{e^2}{a_0}\beta\psi^3 t^2] \tag{2.34}$$

The first term in brackets is the required LDA response to the system. With some algebra, the second term, being zero implies a relation between μ and β such that

$$\mu = \beta\frac{\pi^2}{3} \tag{2.35}$$

fixing the value for μ. The β coefficient for PBE is derived from numerical GGA [15] and has the value ~ 0.066725 resulting in a μ of 0.21951.

This original formalization of the PBE was done in 1996, since then a whole family of functionals have been constructed that take the same form of the PBE but use different values for μ, β, and κ. One such functional is the PBEsol [7]; its μ, β, and κ values are 0.12346, 0.046, and 0.804 respectively. The μ value for PBEsol was chosen as such to reproduce the second-order gradient expansion of E_X. The β value was determined such that the jellium surface energies were accurately produced. These changes improved PBEsol's treatment of solid systems; providing better lattice constants and bulk moduli. Another functional known as APBE [8] uses non-interacting many-electron neutral atoms for its reference system. This produces a different μ value obtained from the modified second-order gradient expansion [16, 17]

and, instead of fixing μ to β, β is the fixed parameter. The μ, β, and κ values for APBE are 0.260, 0.079, and 0.804 respectively. PBE, PBEsol, APBE, and the previously discussed LDA are the functionals of interest within this document.

2.2 Pseudopotentials

Within DFT there are two primary forms of calculating the ground-state properties of the system: all-electron (AE) and pseudopotential (PsP). An AE type calculation takes into account every electron within the system. This form of calculation provides the most accurate result but is the most computationally expensive. For simple systems such as average molecules or free atoms this price of computation has little to no affect. On the other hand, for systems like solids, DNA strands, or hydrocarbon surface catalysis the price becomes prohibitive and even impossible to use an AE calculation. It is in these cases that a PsP would be well suited.

The primary idea of a PsP is to remove the core electrons under the frozen core approximation [9] leaving only the chemical active valence electrons to be dealt with explicitly. This is done under a strict condition that the pseudo-orbitals must match the real orbitals at a set radius (Figure 2.2 and 2.3). This is know as the radius cut-off or r_{cut}. In principle this could be any value one wished, however, large values lead to 'soft' PsP's which tend to decrease accuracy. On the other hand, values too small cause 'hard' PsP's which greatly increase convergence times, removing the advantage gained by the PsP in the first place. It then becomes the task of the user to determine what a 'good' r_{cut} should be.

Because a PsP for a particular atom is based on the AE calculation of that atom, the AE potential of the free neutral atom must first be found for a particular XC functional. Once that is accomplished there are different methods for generating

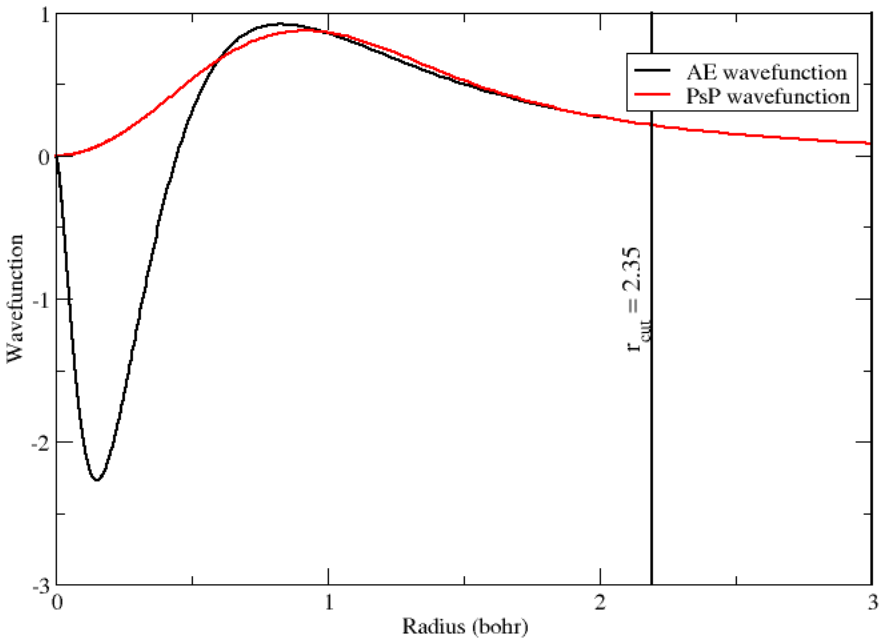

Figure 2.2: The real d valence orbital of Pd compared to its pseudo-orbital. Note that the two orbitals match at the r_{cut} value of 2.35.

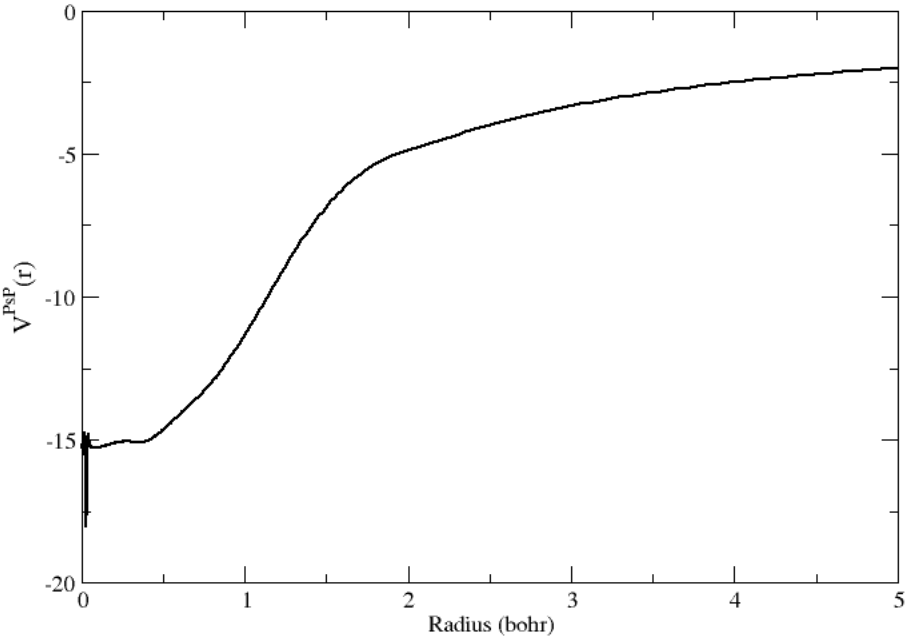

Figure 2.3: Pd pseudopotential for the valence d-state. Used to generate pseudo-orbital.

the PsP: Hamann [18] scheme, Kerker [19] scheme, Vanderbilt [20] scheme for ultra soft PsP's, or Troullier-Martins [21] scheme (used here). The first step is to make the so-called screened PsP that acts as an effective potential on the pseudo-valence states $\Psi_{lm}^{PsP} = [u_l^{PsP}(\epsilon_l^{PsP}; r)/r]Y_{lm}(\Omega_r)$, where the angular momentum l is the lowest eigenfunction of the radial Schrödinger equation

$$\left[-\frac{1}{2}\frac{d^2}{dr^2} + \frac{l(l+1)}{2r^2} + V_l^{PsP,scr}(r) - \epsilon_l^{PsP}\right] u_l^{PsP}(\epsilon_l^{PsP}; r) = 0 \tag{2.36}$$

The pseudo-orbital with angular momentum l, $u_l^{PsP}(\epsilon_l^{PsP}; r)$, will first be derived from the AE valence orbital with angular momentum l such that i) they have the same eigenvalue

$$\epsilon_l^{PsP} \equiv \epsilon_{nl}^{AE} \tag{2.37}$$

ii) the pseudo-wavefunction agrees with the AE wavefunction after r_{cut}

$$u_l^{PsP}(\epsilon_l^{PsP}; r) = u_{nl}^{AE}(\epsilon_{nl}^{AE}; r) \quad for \quad r > r_{cut} \tag{2.38}$$

and is normalized. iii) a norm-conservation constraint is imposed

$$\int_0^{r'} |u_l^{PsP}(\epsilon_l^{PsP}; r)|^2 dr \equiv \int_0^{r'} |u_{nl}^{AE}(\epsilon_{nl}^{AE}; r)|^2 dr \quad for \quad r' \geq r_{cut} \tag{2.39}$$

and finally iv) the pseudo-wavefunction contains no nodes. This is required to obtain a continuous PsP which is regular at the origin, it can be differentiated twice and fulfils the limit $\lim_{r\to 0} u_l^{PsP}(r) \propto r^{l+1}$. Then, manipulating equation (2.36) the respective screened PsP can be pulled out.

$$V_l^{PsP,scr}(r) = \epsilon_l^{PsP} - \frac{l(l+1)}{2r^2} + \frac{1}{2u_l^{PsP}(r)}\frac{d^2}{dr^2}u_l^{PsP}(r) \tag{2.40}$$

This screened potential represents not only the potential caused by the core but also those caused by the electron's XC energy and the Hartree energy. Because of the above conditions this screened PsP will become identical to the AE potential beyond

r_{cut}. This, however, is not the form needed as we are only trying to approximate the core contribution. The final ionic PsP is what is required and can easily be found using the screened PsP:

$$V_l^{PsP}(r) = V_l^{PsP,scr}(r) - V^H[\rho_0^{PsP};r] - V^{XC}[\rho_0^{PsP};r], \tag{2.41}$$

where $V^H[\rho_0^{PsP};r]$ is the electrostatic potential, $V^{XC}[\rho_0^{PsP};r]$ the potential caused by the XC functional, and $V_l^{PsP,scr}(r)$ from equation 2.40. V^H and V^{XC} both require the valence electron density which is evaluated from the pseudo-wavefunctions with the same occupancies as the AE states

$$\rho_0^{PsP} = \frac{1}{4\pi}\sum_{l=1} f_l \left|\frac{u_l^{PsP}(\epsilon_l^{PsP};r)}{r}\right|^2 \tag{2.42}$$

It is important to note that in some cases V^{XC} can be improved upon if we know what the core density is close to the valence peak. This is known as a 'non-linear core correction' and will be touched on in chapter 4.

With the PsP now defined the total energy of an arbitrary system is

$$E^{total} = \sum_i f_i < \Psi_i|T + V^{PsP}|\Psi_i > + E^H[\rho^{PsP}] + E^{XC}[\rho^{PsP}] \tag{2.43}$$

2.3 Methodology

This section will detail the planewave pseudopotential method for solving the electronic systems problem in DFT. Many different coding packages use this method in solving DFT problems, one such package is ABINIT [22, 23] which is what was used for this research. The planewave pseudopotential method uses an iterative process known as a self-consistent calculation to approximate the solution. Within this process there are five primary steps (Figure 2.4). The first is to make an educated initial

guess for the ground-state density as a function of position. Next, calculate the effective potential caused by this density under the condition that the KS energy, $E_{KS}[n]$ is minimized with respect to the density (see eq. 2.11 and following)

$$V_{KS} = \frac{\delta E_{ext}}{\delta n(\mathbf{r},\sigma)} + \frac{\delta E_H}{\delta n(\mathbf{r},\sigma)} + \frac{\delta E_{XC}}{\delta n(\mathbf{r},\sigma)} = V_{ext} + V_H + V_{XC}. \tag{2.44}$$

Here V_{XC} contains the information about the XC functional in use. Next, take this effective potential and plug it into the KS Hamiltonian (eq. 2.15)

$$\left[-\frac{1}{2}\nabla^2 + V_{KS}\right]\Psi_i = E_i\Psi_i \tag{2.45}$$

Next, the wavefunctions can be found which, in turn, will provide the density as a function of position.

$$n(r) = \sum_i |\Psi_i(r)|^2 \tag{2.46}$$

If this new density is equal to the initial density to within a tolerance level, then the calculation is done and the ground state energies are calculated using equation (2.9). If it is not, however, then this new density is used to find a new effective potential and the cycle continues until convergence is reached.

Atoms, molecules, and solids are all constructed in a planewave code as a system of periodic cells. This allows for the application of the Bloch theorem: eigenfunctions of the wave equation are the product of planewaves.

$$\Psi_{ik} = \mu_{ik}(\mathbf{r})e^{i\mathbf{k}\cdot\mathbf{r}} \tag{2.47}$$

where i is the electron band number, $\mathbf{k}$ is the wave vector, and μ_{ik} is a function that has the same periodicity of the system. One can expand μ_{ik} as a set of planewaves:

$$\Psi_i(\mathbf{r}) = \sum_G c_g^k e^{i(\mathbf{k}-\mathbf{G})\cdot\mathbf{r}} \tag{2.48}$$

where $\mathbf{G}$ is a vector that obeys the periodic boundary conditions of the cell

$$\mathbf{G}\cdot\mathbf{T} = 2\pi M \tag{2.49}$$

where $\mathbf{T}$ is the lattice vector and M is an integer. Because this calculation is implemented within a computer and there is an infinite number of possible G values, a cut-off needs to be imposed:

$$\frac{\hbar^2}{2m}\mathbf{G}_{max}^2 = E_{cut}. \tag{2.50}$$

The value E_{cut} is discussed in greater detail in section 3.1. The density now takes the form of a summation over the orbitals integrated over all k-space:

$$n(\mathbf{r}) = \sum_i \int \frac{d^3k}{(2\pi)^3} |\Psi_{ik}(\mathbf{r})|^2 \tag{2.51}$$

The number of orbitals to be summed is already limited by $\mathbf{G}_{max}$ but k is a continuous variable over all k-space which needs to be limited for computational implementation. The first limit is found in k's periodic nature and only those k values within the Brillouin zone (BZ) will provide unique information [24]. Now we only need to integrate over the BZ, however we still have a continuous k. This is solved using the classic mathematical approach to integration; breaking it up into finite segments. The more segments used and the smaller the segment, the more accurate the value for the density will be. As the number of finite chunks of k-space increases, there will be a point where the increase in accuracy will greatly diminish. At this point the density can be considered converged. These minimized 'grids' in k-space have been implemented by Monkhorst and Pack [25] as well as used in ABINIT [22, 23]. There are now two variables which control the accuracy of the self-consistent calculation based on planewaves, the chunks of k-space and the number of planewaves used. How these values are implemented within ABINIT will be discussed in chapter 3

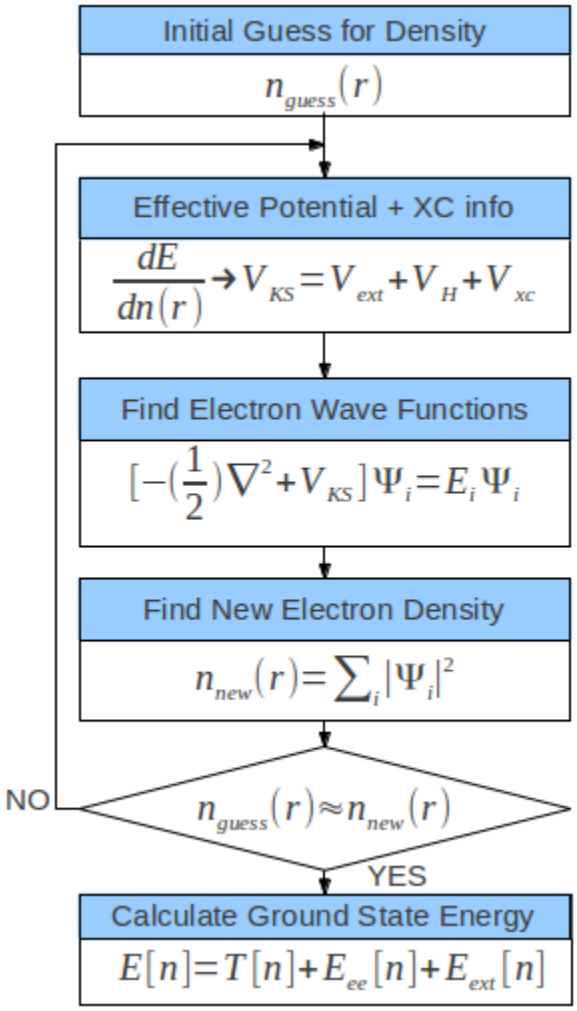

Figure 2.4: This flow chart details the self-consistent calculation used within ABINIT to solve the electronic system problem

Chapter 3

Solid Test Set

3.1 Solid Systems

The primary goal of this research is to address the quality of XC functionals created in an AE environment used within a PsP environment for solids. A set of 16 different simple solids have been chosen, covering a large range of material types, to investigate this goal. Within this chapter the systems will be described, important convergence properties addressed, and target measurements detailed.

3.1.1 The 16 Solid Test Set

The solids can be broken up into four categories: simple metals, semiconductors, ionic compounds, and transition metals. Li, Na and Al are the simple metals; C, SiC, Si, Ge, GaAs are the semiconductors; NaF, NaCl, LiF, and LiCl are the ionic compounds; finally Cu, Rh, Pd, and Ag are the transition metals. The structural type along with the experimental values for the ground-state properties lattice constant, bulk modulus, and cohesive energy can be found in Table 3.1.

Table 3.1: List of the test set with structure type, experimental lattice constant, bulk modulus, cohesive energy and zero point energy

Solid	Structure	a_0^{Expt} [26] (Bohr)	B_0^{Expt} [26] ($10^{11} N/m^2$)	$E_{cohesive}^{Expt}$ [27] (Ha)	E_{ZPE} (Ha)
Li	bcc	6.573	0.13	0.060	0.00123
Na	bcc	7.987	0.075	0.041	0.00056
Al	fcc	7.622	0.794	0.125	0.00152
C	diamond	6.743	4.43	0.544	0.00794
SiC	zincblende	8.223	2.25	0.468	0.00428
Si	diamond	10.265	0.992	0.340	0.00228
Ge	diamond	10.684	0.758	0.284	0.00132
GaAs	zincblende	10.677	0.756	0.247	0.00123
NaCl	cubic	10.577	0.266	0.239	0.00114
NaF	cubic	8.713	0.514	0.278	0.00175
LiCl	cubic	9.652	0.354	0.256	0.00150
LiF	cubic	7.580	0.698	0.320	0.00261
Cu	fcc	6.811	1.42	0.128	0.00122
Rh	fcc	7.180	2.69	0.212	0.00171
Pd	fcc	7.336	1.95	0.143	0.00098
Ag	fcc	7.692	1.09	0.108	0.00080

3.1.2 Convergence Calculations

Each solid is implemented within the DFT code ABINIT using an input file unique to that system. In order to maintain consistent results, each system has to be checked for energy convergence. This is done by examining three properties of the ABINIT calculation: maximum planewave kinetic energy allowed (E_{cut}), smearing of electron occupations (T_{smear}), and the fineness of k-space sampling grid (N_{kpt}). Under atomic units where

$$\hbar = e^2 = m_e = 1 \tag{3.1}$$

giving length in Bohr and energy in Hartree, a planewave kinetic energy is directly related to its wave number

$$E_{cut} = \langle KE \rangle = \frac{k^2}{2} \tag{3.2}$$

Then enforcing E_{cut} not only limits the energy but also the total number of planewaves used for the calculation. To determine what value needs to be used for a particular system in order to be considered converged, E_{cut} is varied and the total energy of that system is found. These values are then plotted to find a point when the change between point to point is less thqn 0.001 Ha (Figure 3.1).

The fineness of the k-space sampling grid within the first BZ is defined by the three valued parameter N_{kpt}. For the majority of the solids this is the last parameter that needs to be converged with respect to the energy. This is done using the same method as for E_{cut}: change N_{kpt}, get the total energy for the system, and plot them to find a converged value (Figure 3.2). A few systems, like metals, also require the smearing, or broadening of occupation states done by the temperature of smearing value T_{smear}. This allows the electrons to shift between occupide and unoccupide states at the Fermi level in the search of total energy minimization. For the systems within the test set that require it, T_{smear} must be converged in conjunction with N_{kpt}

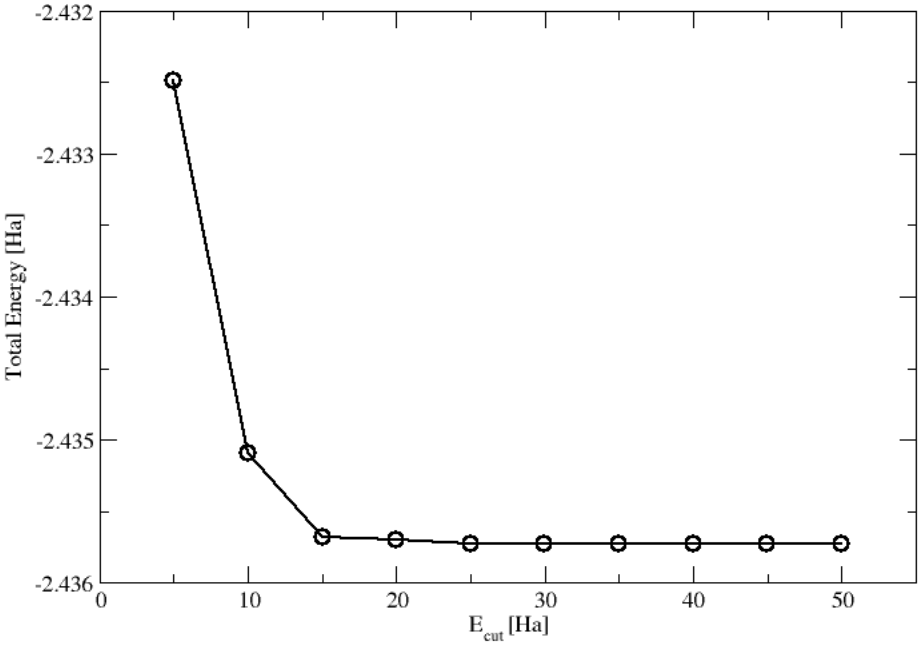

Figure 3.1: Energy convergence for the E_{cut} in Al. The convergent value selected from here is 20 Ha

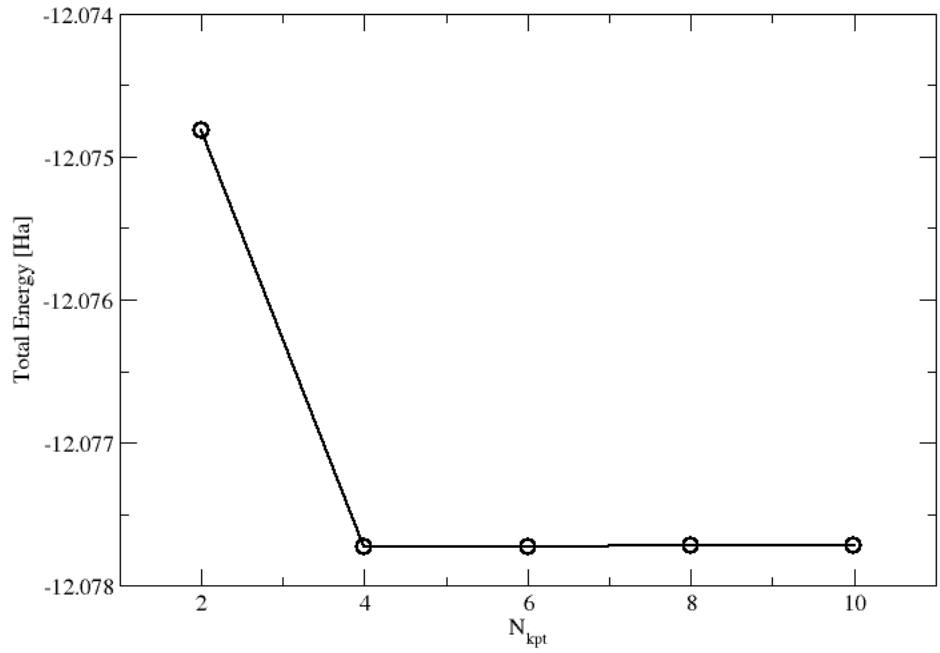

Figure 3.2: Energy convergence for the N_{kpt} in C. The value selected from here is 6 6 6

(Figure 3.3).

A complete list of converged values can be found in Table 3.2. Along with the solid systems, the free neutral atomic systems are required for later calculations. For more information on the free systems refer to section 3.2.5.

3.1.3 False Convergence

Seen primarily with transition metals is the effect of false or very slow convergence. Even though this effect can cause only small energy differences ($\Delta E \sim 0.0006 Ha$ for Rhodium) it is important to know of its presence. The system where this effect is most apparent is Copper (Figure 3.4). An early E_{cut} convergence value for Copper was 45 Ha, however, the true convergence value is out at 75 Ha. The difference between the

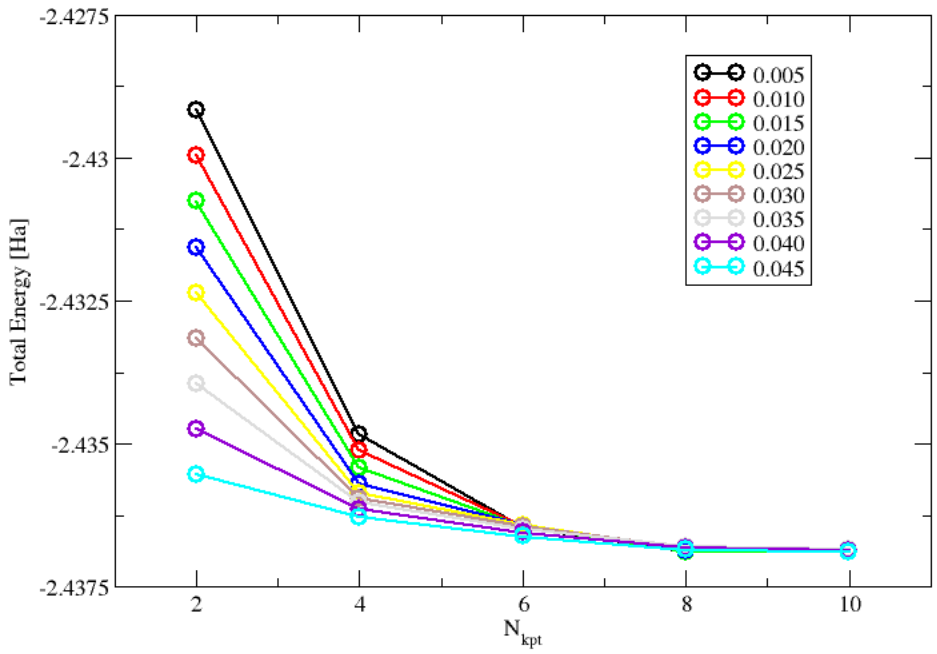

Figure 3.3: Energy convergence for the T_{smear} and N_{kpt} in Al. Each data set is at a different T_{smear} ranging from 0.005 to 0.045. The values selected are $T_{smear} = 0.035$ and $N_{kpt} = 6\ 6\ 6$

Table 3.2: Converged ABINIT input parameters for the test set. Those with no T_{smear} value do not require occupation broadening

Solid	E_{cut} (Ha)	N_{kpt}	T_{smear} (Ha)
Li	17	6 6 6	0.015
Na	15	6 6 6	0.020
Al	20	6 6 6	0.035
C	25	6 6 6	—
SiC	50	6 6 6	—
Si	25	4 4 4	—
Ge	50	6 6 6	—
GaAs	40	6 6 6	—
NaCl	38	2 2 2	—
NaF	65	4 4 4	—
LiCl	32	4 4 4	—
LiF	50	4 4 4	—
Cu	75	8 8 8	0.020
Rh	50	6 6 6	0.025
Pd	50	8 8 8	0.030
Ag	75	8 8 8	0.020

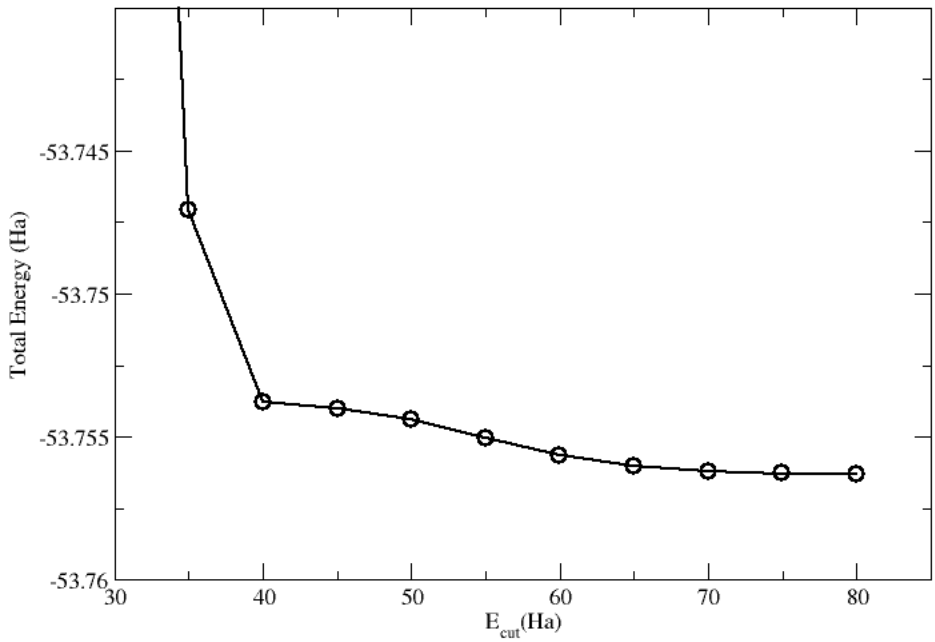

Figure 3.4: The Copper energy cut-off convergence plot, zoomed in to show the false convergence found at 45 Ha. The better value is at 75 Ha. The is difference ~ 0.0025 Ha in total energy and produces better results.

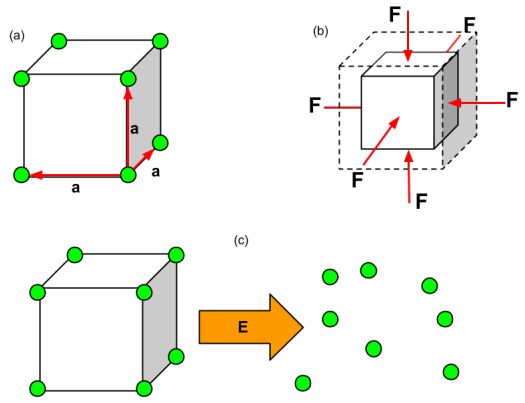

Figure 3.5: Graphical representations of the three target ground state properties. a) the lattice constant; distance between two nearest neighbours. b) bulk modulus; solid's response to uniform external pressure. c) cohesive energy; amount of energy to convert bulk crystal to free, neutral atoms

total energies of these two cut-offs is $\Delta E \sim 0.0025\ Ha$ which is over twice the size of the convergence condition $< 0.001\ Ha$.

3.2 Test Set Measurements

As stated within 2.1 a self-consistent calculation outputs the ground-state energy of an electronic system. Along with this property, ABINIT also outputs the ground-state lattice constant of the system. Using these two provided values, three important solid ground-state properties can be calculated. The target properties are lattice constant, bulk modulus, and cohesive energy. Below the method for finding each one of these properties is detailed.

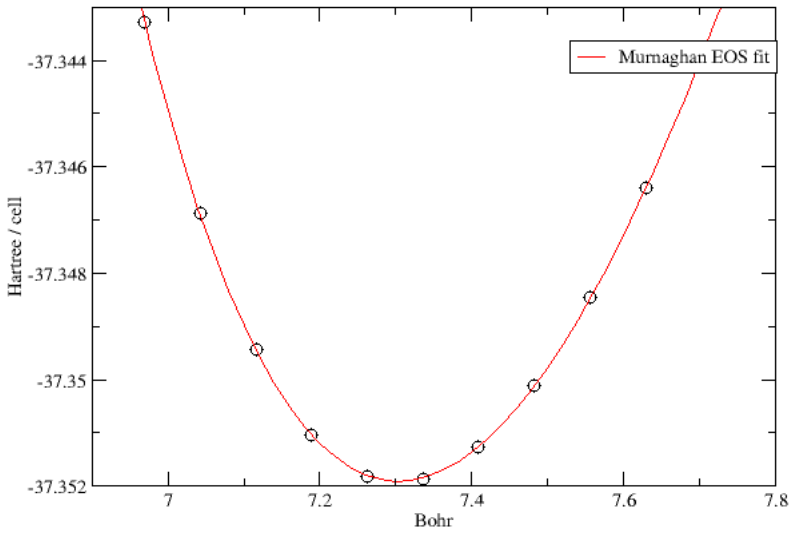

Figure 3.6: Murnaghan equation of state fit for Palladium with the XC-functional LDA. The red line is the fit where the black circles are the data points for Palladium.

3.2.1 Lattice Constant and Bulk Modulus

The lattice constant is the distance between two nearest neighbours within the simplest cubic cell of a crystal (Figure 3.5a). The bulk modulus is a crystal's response to external pressures (Figure 3.5b). This uniform pressure could be positive (pushing in on the crystal) or negative (pulling out). The method used here allows both of these properties to be found simultaneously.

Fixing a system's lattice constant at a particular value is effectively applying a uniform pressure and the solid's response is reflected in the total energy. Doing this for multiple lattice values and plotting the total energy of the solid at that value, a curve is constructed. This curve can be fit to using the Murnaghan equation of state (discussed below). This fit (Figure 3.6) then provides the bulk modulus and the minimum lattice constant value for the solid.

3.2.2 Murnaghan Equation of State

State variables of a system such as temperature, pressure, volume, energy and entropy can all be related to one another with an equation of state. A very simple version of this would be the Ideal Gas Law relating volume and pressure to temperature and quantity of material in a gaseous system. The systems with the test set presented here are solids so the equation of state will need to relate the state variables of pressure, volume, energy, and bulk modulus. Starting with the bulk modulus and drawing on thermal physics it can be written as

$$B = -V\left(\frac{dP}{dV}\right) \tag{3.3}$$

As detailed above the bulk modulus is a solids response to external pressures. This can be also be defined using the Murnaghan equation of state [28] giving the bulk modulus as a function of pressure

$$B(P) = B_0 + B'P \tag{3.4}$$

where B_0 is the bulk modulus at zero pressure and $B' = \frac{dB}{dP}$. An equation for P can be found in terms of V

$$P = \frac{B_0}{B'}\left[\left(\frac{V_0}{V}\right)^{B'} - 1\right] \tag{3.5}$$

at constant entropy the pressure is related to the energy of the system

$$P = -\frac{dU}{dV} \tag{3.6}$$

so(3.5) is now

$$dU = -\frac{B_0}{B'}\left[\left(\frac{V_0}{V}\right)^{B'} - 1\right]dV \tag{3.7}$$

V_0 has now become the volume at minimum energy. Integrating to get the system energy as a function of volume

$$U(V) = U_0 - \frac{B_0}{B'}\left[\int\left(\frac{V_0}{V}\right)^{B'} dV - \int dV\right] \tag{3.8}$$

Solving the integrations and applying some substitutions

$$U(V) = U_0 - \left(\frac{B_0}{B'}V_0\right)\left[\frac{\left(\frac{V_0}{V}\right)^{B'-1} - 1}{1 - B'} - \frac{V_0}{V} + 1\right] \tag{3.9}$$

Now $U(V)$ can be used as a fitting function with four fitting parameters: U_0 the minimum energy, V_0 the minimum volume, B_0 the bulk modulus, and B' the first pressure derivative of the bulk modulus. It is important to remember that we are not interested in the volume of a system but its lattice constant. Luckily, these two parameters are related simply by $V_0 = a_0^3$ for the simple cubic, $V_0 = \frac{1}{2}a_0^3$ for the body-centered cubic, and $V_0 = \frac{1}{4}a_0^3$ for the face-centered cubic. All of these values can then be retrieved from any solid system by fitting a plot of total energy versus lattice constant with $U(V)$.

3.2.3 Cohesive Energy

The cohesive energy is the amount of energy required to decompose a crystal to neutral isolated atoms. This, however, would be infinite for crystals within ABINIT as they have periodic boundary conditions making them infinite structures. In order to avoid this infinity, cohesive energy will be considered per unit cell. To calculate this, first the bulk system's total energy per unit cell is found using the minimized lattice constant found from the Murnaghan equation of state. Then the total energy of the free atomic system is found; in the case of diatomic systems two total energies are found. For more information on atomic data please see section 3.2.5. Then a zero point energy (energy of phonon vibrations at zero temperature) is also calculated for the system. The equation can then be written as

$$E_{cohesive} = \sum_{n=1}^{N} E_n^{free} - E_{bulk} - NE_{ZPE} \tag{3.10}$$

where N is the number of atoms in the primitive cell. The zero point energy (ZPE) per atom, E_{ZPE} is calculated from the following equation

$$E_{ZPE} = \frac{9}{8} k_b \Theta_D \tag{3.11}$$

where Θ_D is the Debye Temperature [24]. Theoretical values for the cohesive energy are in Table 3.1 along with the ZPE values.

3.2.4 Experimental Cohesive Energy

Two primary sources have been used for the experimental cohesive energy values: Kittel's text on solid state physics [24] and the JANAF thermal physics tables [27]. It is very important to note how the values are reported in order to match them with our results. In both texts, for any system with only one atom they report the same, but for diatomic systems that is not the case. For the JANAF tables, a cohesive energy value is calculated using [29]

$$\Delta_f H^0_{0,ideal} = \Delta_f H^0_{298.15K} + (H^0_0 - H^0_{298.15K})_{gas} - (H^0_0 - H^0_{298.15K})_{crystal} \tag{3.12}$$

where $\Delta_f H^0_T$ effectively means the standard-state enthalpy of formation of the gas from crystal at temperature T. Standard-state is denoted by the 0 superscript and means that the system is held at 100,000 Pa. Qualitatively, the equation stands for the amount of energy to take a crystal composed of element **A** to neutral isolated atoms **A**. For all systems in the JANAF tables this value is reported and can be found under the ideal gas section for that substance. Equation (3.12) also assumes that the bulk crystal is the zero reference energy. For systems where this is not the case, such as diatomic systems, (3.12) needs to be shifted by the ΔH of formation of the crystal

$$\Delta_f H^0_{0,cohesive} = \Delta_f H^0_{0,ideal} - \Delta_f H^0_{0,crystal} \tag{3.13}$$

This will provide the correct value for the cohesive energy of a diatomic system. To better understand what (3.12) and (3.13) mean for a diatomic system, an example calculation is presented for NaCl. The ΔH of formation of the crystal for NaCl is -410.693 kJ/mol and the ΔH of formation of the ideal gas is -180.425 kJ/mol. This provides a value of $\Delta_f H^0_{0,cohesive} = 230.268$ kJ/mol. This means that it takes 230.268 kJ/mol (or 0.087 Ha) to take NaCl crystal to NaCl gas.

This is an important outcome as it was found not to be the same as our theoretical calculation for the cohesive energy. In order to match the JANAF tables for any diatomic system our calculation would have to be adjusted to calculate the molecular dimer energies. For three of the six diatomic systems this was done to show that we could match with JANAF if need be. The results from the adjusted calculation are found in Table 3.3. The Theoretical calculation is almost the same as before, however the ZPE needs to be adjusted to account for the molecule still having one bond to vibrate. This bond will reduce the ZPE of the system by

$$E^{mol}_{ZPE} = \frac{1}{2} k_b \Theta_D$$

, resulting in a new ZPE

$$E'_{ZPE} = E_{ZPE} - E^{mol}_{ZPE} = \frac{5}{8} k_b \Theta_D$$

From Kittel, the cohesive energy for a diatomic system is reported as the amount of energy to take the crystal to isolated ions per unit cell. Once again, this is not the same as what we are calculating as the cohesive energy, however it can be converted. To make the values match, the amount of energy to make $Na^+ \rightarrow Na$ (ionization potential) and $Cl^- \rightarrow Cl$ (electron affinity) needs to be added to Kittel's. Doing so changes Kittel's reported value to the amount of energy to take a crystal to isolated

Table 3.3: The cohesive energy calculations for diatomic systems. The energy represents the amount of energy to break the crystal up to neutral isolated diatomic particles.

Solid	LDA (Ha)	Experimental [27] (Ha)	% Diff
NaCl	0.0969	0.0877	10.52
LiCl	0.1132	0.1033	9.60
LiF	0.0887	0.0811	9.36

neutral atoms per unit cell, which is what we are calculating (Eq 3.10). As this change only affects the experimental value (which is calculated only once), these values are what is used for the diatomic systems and are reported along with the monatomic system values from JANAF in Table 3.1.

3.2.5 Atomic Data

As stated above, in order to calculate the cohesive energy for a bulk system, the free atomic system energies need to be found. This is also done using ABINIT, but configured for a free neutral atom. These systems also need to be converged with respect to energy for two parameters, E_{cut} and a_{cell}. The E_{cut} convergence is the same as detailed in section 3.2. The atomic cell, or a_{cell} controls the size of the simulated region. For solids, a_{cell} is synonymous with the lattice constant; for free atoms it is the space that the atom occupies. It must be large enough to prevent atomic orbitals from overlapping, maintaining the condition of being a free atom. The convergence is similar to that of E_{cut}; increase the size until total energy convergence. All the converged values for the atomic systems are listed in Table 3.4. It is important to the note the valence configuration for Pd. The true ground state system of Pd has a valence structure of $4d^{10}$, however, it has been found that in order to have solid type bonding it must be in a configuration of $4d^9 5s$ (notes on issues with atomic orbitals

Table 3.4: Converged ABINIT input parameters and valence electron structure for the free atoms that compose the solid test set.

Solid	Valence Electrons	E_{cut} (Ha)	a_{cell} (Bohr)
Li	2s	15	28
Na	3s	15	26
Al	$3s^2 3p$	50	22
C	$2s^2 2p^2$	35	20
Si	$3s^2 3p^2$	35	20
Ge	$4s^2 4p^2$	40	30
Ga	$4s^2 4p$	35	25
As	$4s^2 4p^3$	35	25
Cl	$3s^2 3p^5$	35	18
F	$2s^2 2p^5$	45	15
Cu	$3d^{10} 4s$	50	28
Rh	$4d^8 5s$	50	26
Pd	$4d^9 5s$	45	28
Ag	$4d^{10} 5s$	80	40

in ABINIT can be found in appendix C).

Chapter 4

Testing Pseudopotentials

This chapter will focus on three topics: PsP libraries, reproducing and testing the libraries, and comparing our own PsP scheme with the libraries. When looking at PsP libraries we will discuss where to locate them, what they have available, and their limits. Because of a lack of coverage for new GGA's in some libraries, the need to make our own becomes important. We will start by reproducing the library PsP's discussing the types of information needed to create a PsP. Any differences between our PsP's and the ones from a library will be discussed along with a need to make our own scheme.

4.1 Pseudopotential Libraries

An important aspect to the planewave pseudopotential method for solving the electronic system is developing a PsP to use that accurately represents the systems in question. There are many resources available to researchers in need of PsP's that may not have the time or ability to make their own. The National Nanotechnology Infrastructure Network (NNIN) [30] is one such resource with information on

DFT coding packages, PsP libraries, PsP generating coding packages, and the like. They also provide a PsP 'search engine' that will find PsP's for a particular element, display the XC functional used, the file format, and the library that the PsP is located in. The PsP library originally used for this research was the one provided by ABINIT, located on their website (http://www.abinit.org/downloads/psp-links). This library was chosen over the others because it was connected to ABINIT, the DFT code used in this research. The XC functional categories within this library are LDA and GGA. Under LDA is a list of PsP's for almost all elemetns created using the Troullier-Martins scheme and a handfull of PsP's created using different schemes. Under the GGA category, the primary XC functional provided is the PBE also under the Troullier-Martins PsP scheme. One limitation of this library is the lack of PsP's generated with more recent GGA functionals. As this research focuses on four different XC functionals (LDA, PBE, PBEsol, APBE), PsP's of the same type are needed (it is possible, however, to mix one type of PsP with a different type of DFT calculation. What happens in this case will be answered in chapter 5).

Because the ABINIT library does not contain all the needed PsP's for this research we need to build our own. An important aspect of this venture will be making sure that our PsP's are providing accurate results. We tested this by making PsP's from information found within the ABINIT library about their PsP's. Before we dive into the results of this test, we first need to understand what things are needed by a PsP generating code in order to make a PsP.

4.1.1 Generating Custom PsP's

As already discussed in section 2.2, a PsP is based off of the real potential from an AE calculation. The AE calculation needs to know four things: atomic number, wave

equation, all the electron orbitals and the XC functional. As detailed previously, the Schrödinger wave equation was the first used to generate a PsP but there are additional options including the Dirac wave equation and scalar-relativistic wave equation. The Dirac wave equation is a generalization of the Schrödinger equation in a relativistic form. The scalar-relativistic equation is a reformulation of Dirac's equation where an averaging is done over the total angular momentum quantum numbers to remove the equation's dependency on them. As a consequence, it includes relativistic effects except for spin-orbit coupling. A more detailed description of these equations can be found in Richard Martin's text *"Electronic Structure"* chapter 10 [11]. From these choices an AE calculation is performed on the free system generating information to be used in the PsP calculation.

The most important, user defined information needed to perform a PsP calculation is what makes up the valence electrons of the system. Four things need to be known about a valence orbital: the quantum numbers n and l, the PsP scheme to be used (Troullier-Martins, Hamann,...), and the radial cut-off. As detailed in section 2.2 the radial cut-off or r_{cut} is the point at which the real orbital matches the pseudo-orbital. Anything within this r_{cut} is approximated under the PsP method.

A calculation using a PsP normally depends on just the valence density and in the majority of cases this is an adequate approximation. However, in some cases explicit information about core-valence interactions is needed. For example, Lithium's inner 1s overlaps slightly with the outer 2s (figure 4.1). This causes interaction between the two which would be missed (especially by the XC energy) if the core was completely removed. Because the overlap is small, only a core correction to the system is needed. This can be accomplished by adding in a so-called partial-core density which reproduces the true core density but is a smoother function, which enables its use with planewaves. This core correction effectively raises the potential

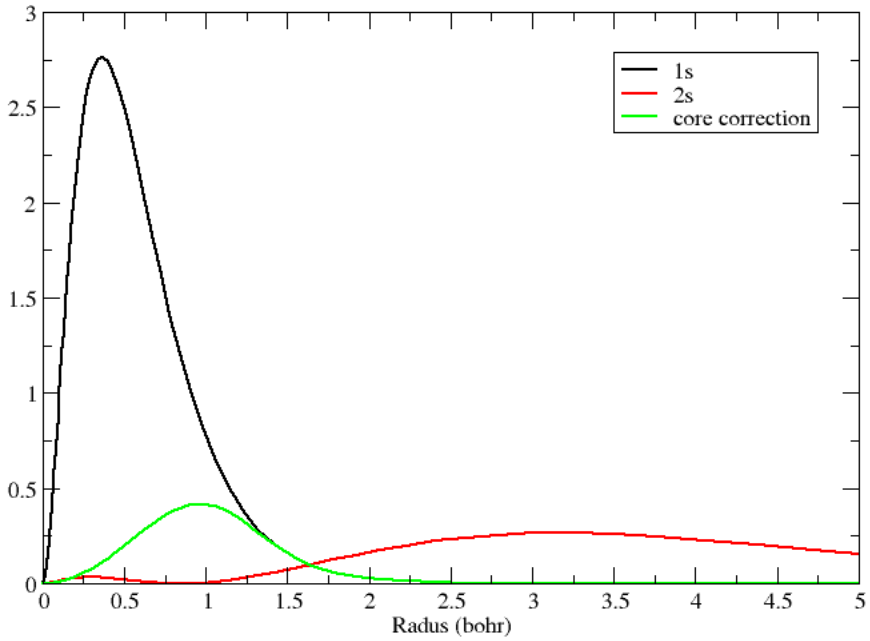

Figure 4.1: This plot of the Lithium 1s and 2s orbital probabilities show how they have an overlap. This interaction causes the need for a core correction for the PsP which is also plotted

in the core and smooths it out (figure 4.2). In those cases where a core correction would not be enough, such as the 3d orbital of Gallium (figure 4.3), the offending shell is completely added to the valence.

A list of the more commonly available PsP generating packages that require the above information can be found on the NNIN website on their "Virtual Vault for Pseudopotentials and PAW Datasets" page. One package we could have chosen to use was the fhi98PP package [31]. This is the same code used by ABINIT to generate the PsP's listed in their library, however this package is no longer maintained, with the last major update being in 2003. The package that was chosen here is the Atomic Pseudopotential Engine (APE) [32]. It is well maintained, currently on build 2.1.0 last updated in 2013, and has an active user forum frequented by the creators for

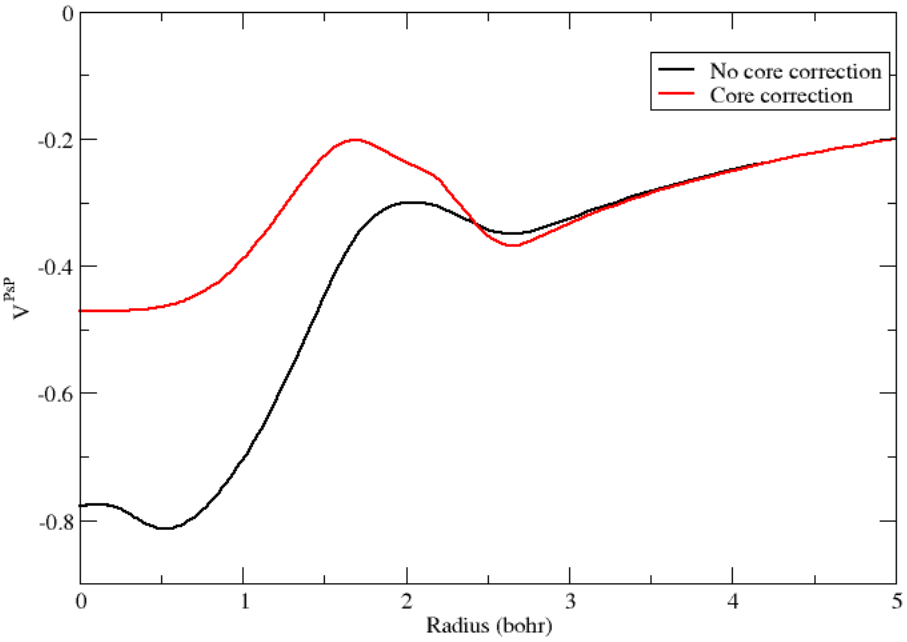

Figure 4.2: The p-state PsP of Na using the PBE XC functional both with core correction and without. The core corrected one has a higher potential within core region.

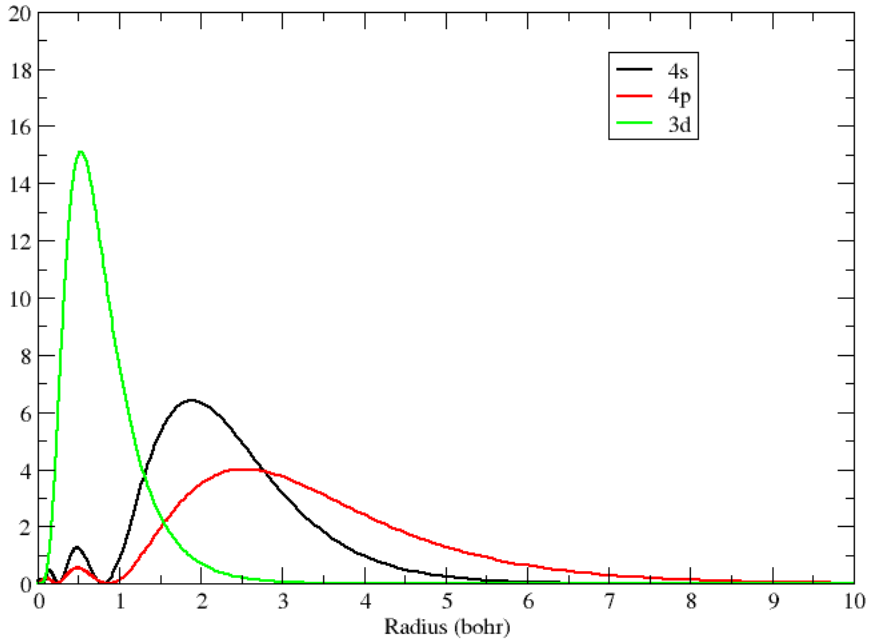

Figure 4.3: This plot shows the two valence orbital probabilities of Gallium;4s and 4p and a semi-core orbital; the 3d. Because the 3d extends so far out into the valence a core correction is not enough and it has to be added in as a valence state.

active debugging and solution finding. APE is also designed to work with the code library libXC [5], an archive of XC functionals for DFT. LibXC's goal is to provide a portable, well tested and reliable set of XC functionals for the use in all DFT coding packages. Currently there are over 300 functionals within the library including those needed for this research. Conveniently, ABINIT is also able to use libXC allowing access to all the functionals.

4.1.2 Testing Pseudopotential Libraries

Now that we have an understanding of what a PsP coding package needs, we can collect that information and attempt to match the results of the ABINIT PsP's. Which elements require core corrections, the type of wave function used and the valence orbitals included can all be gleaned from the provided ABINIT PsP input and output files. The one piece of information missing is the radial cut-off value. Through extensive searching it was found that another coding package called SIESTA [33] was built using information from the ABINIT library and had reported the r_{cut} values. With all this information we built PsP's and found the lattice constant values for them.

The lattice constant results for the PsP's generated with APE using the SIESTA cut-offs and the ABINIT library PsP's are plotted in figure 4.4 as the percent difference from experiment and are labelled 'SIESTA' and 'ABINIT' respectively. For seven of the fourteen solids used in this test, the two data sets match fairly well, however, they are not an exact match as we had expected. As the wave equation, orbitals, and core correction information came directly from ABINIT, the only thing that could have been wildly different, besides the coding package, was the r_{cut} values from SIESTA. This launched another investigation into the r_{cut} values used by the

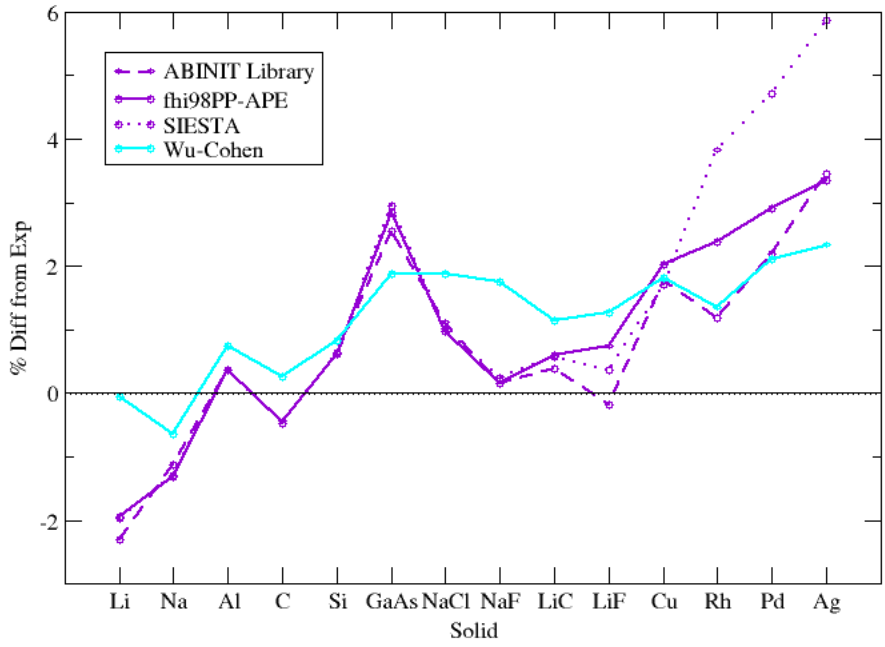

Figure 4.4: These lattice constant results for PBE are reported as percent difference from experiment. Each data set uses a different method for making the PsP's.

ABINIT library.

Fhi98PP, the coding package used to generate the ABINIT PsP library, self-generates the r_{cut} values unless otherwise specified. Because of this, no input files provided by ABINIT contains this information. Upon investigating fhi98PP directly, the values used were extracted from the code. This allowed us to perform another solid test using these new values. These lattice results, labelled 'fhi98PP-APE', are also plotted in figure 4.4. Once again for seven of the systems the data sets match, however, even with the r_{cut} values from fhi98PP used, we can not reproduce all of the ABINIT results. The solids that disagreed the most are the ionic compounds and transition metals.

Focusing on the transition metals, both the 'fhi98PP-APE' and 'SIESTA' data sets

show the same trend, deviating more from experiment moving from Cu to Ag. This trend is not followed by the 'ABINIT' data set which dips for Rh. This suggests that there is something different about their treatment of Rh and possibly all transition metals. Looking into the provided ABINIT PsP input file for Pd shows that the empty p-orbital was give an artificially high eigenvalue so it would not be accessible to the solid system for bonding. Doing so favoured the true s- and d-bonding of the Pd solid but this type of adjustment is not possible within APE. In fact all transition metals within the ABINIT PsP library have this adjustment to the empty p-state.

In an attempt to achieve the same effect as seen in the ABINIT results, we adjusted the r_{cut} of the empty p-state and plotted it against the resulting lattice constant values (figure 4.5). As the r_{cut} gets smaller from 3.00 bohr to 2.50 bohr the net change in lattice constant is minimal, however, at 2.25 bohr the lattice constant dramatically drops. The lattice constant at an r_{cut} of 2.25 bohr is 7.16 bohr which is well below the experimental value of 7.336 bohr. In order for the experimental value to be produced an r_{cut} of approximately 2.45 bohr would be needed, however, this falls within the region of fastest change on the lattice constant versus r_{cut} plot. This suggests that the system is not stable and would be a poor choice.

The reason as to why the plot has a jump between 2.25 and 2.50 bohr can be explained by looking at the pseudo-orbital plots (figure 4.6). Because a pseudopotential is required to have no nodes within the pseudo-wavefunction and as r_{cut} gets closer to the outer-most node of the real orbital, the pseudo-orbital starts to become more repulsive in the centre. When this happens the p-orbital is no longer favourable for bonding which results in the smaller lattice constant values. This effect is discussed further in section 6.1.2.

For the ionic compounds, LiF has the largest spread in the results. Looking into the r_{cut} values for Li, the 2s orbital of the 'APE' data set is 2.18 bohr where as

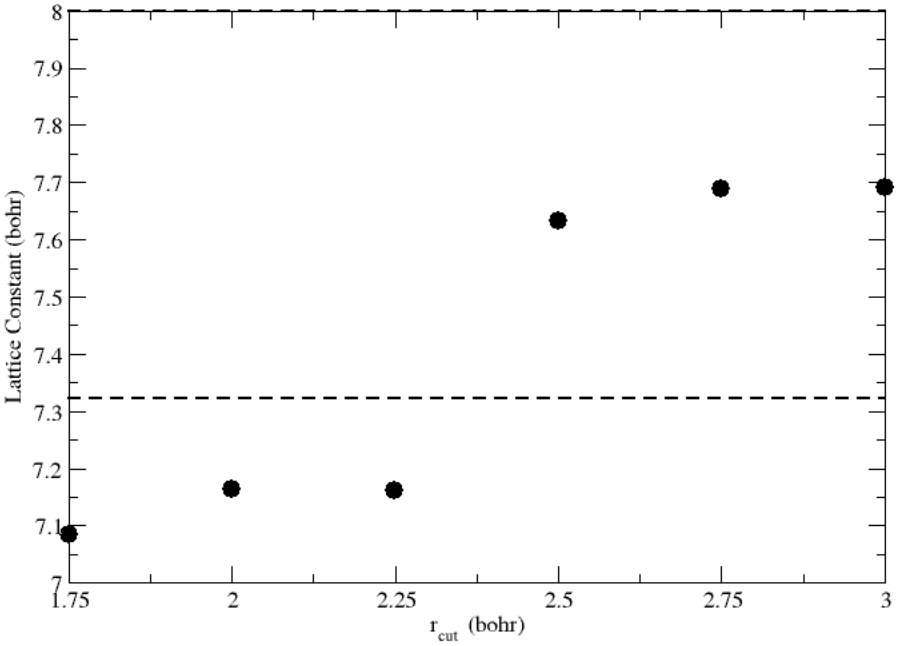

Figure 4.5: The r_{cut} used for the empty p-state and the the resulting lattice constant are plotted. The experimental value (noted by the dashed line) falls within the region of fastest change (2.25-2.50).

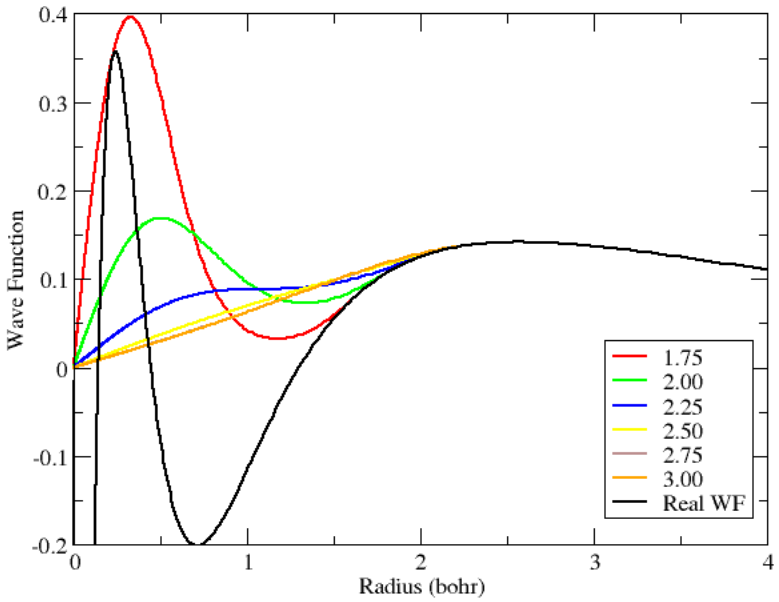

Figure 4.6: The p pseudo-orbital of Pd generated with different r_{cut} values. Note how the pseudo-orbital develops a 'hump' as the r_{cut} gets closer to the first node of the real orbital.

the 'SIESTA' data set has it at 2.28 bohr. For F the 2p orbital has an r_{cut} of 1.34 bohr for 'APE' and 1.41 bohr for 'SIESTA'. We can infer that, because as the r_{cut} value increases the lattice constant increases for LiF, that the 'ABINIT' data set r_{cut} must be even larger. This raises a important question: do we use an r_{cut} value that provides an answer close to experiment, or do we use one that is designed to balance the efficiency and transferability of the PsP?

To help answer this question we added a fourth data set called 'Wu-Cohen' [34] to figure 4.4, another study into PsP's that worked hard and mostly succeeded to match AE results. We can now see that the ABINIT library PsP's for Li and F provide a good result in terms of experiment, but a poor result in terms of matching the AE calculations. Because the goal of this research is to measure how well GGA's perform in a PsP environment, we want to match AE theory as closely as possible; we want any disagreement with experiment to be caused by the functional chosen, not the PsP used. It is for this reason that we stick with the r_{cut} values in the 'APE' data set as ABINIT has adjusted their PsP to provide better experimental results.

Even with the question about which r_{cut} is better, there is still the question as to why the 'APE' data set is still off from the more accurate 'Wu-Cohen' set. There must be an effect taking place within these ionic compounds that our PsP's are unable to account for. Through a literature search a possible culprit was found: core polarization. What is and causes core polarization will be discussed in detail within section 6.1.1.

4.2 Consistent PsP Scheme

The above discussion shows the importance of having a consistent scheme so everything is comparable on the same level. This will also help eliminate many possible

variables that can effect the ending ground-state values. A major concern in regards to PsP's is what to consider valence electrons and what to treat as core. Here, the valence electrons are selected to match with those used from the atomic data calculations detailed in section 3.2.5. In addition to these filled and semi-filled orbitals, one (in some cases two) higher empty orbitals are included to insure convergences. Each of these orbitals have an associated radial cut-off, r_{cut} value. The value selected is the one automatically generated by the fhi98PP coding package. These values are designed to provide a reasonable compromise between PsP transferability and efficiency. The r_{cut}'s and the valence orbitals for each element are listed in table 4.1.

The next choice effects how the PsP is calculated by changing the wave equation used. The scalar-relativistic wave equation is selected here to provide better results for heavier elements that are influenced by relativistic effects without the use of fully relativistic PsP's. Finally, the inclusion of core corrections are applied to two elements: Li and Na. Out of the test set, these are the only elements noted in the fhi98PP documentation to require a core correction for the reasons detailed above (section 4.1.1).

Under these conditions all PsP are generated, one for each element for each XC functional used. These PsP's are in turn used within ABINIT to calculate the ground-state properties of the test set. Raw lattice constant, bulk modulus, and cohesive energy are reported in appendix B.

Table 4.1: Valence orbitals and radial cut-off values for all the elements in the test set generated by fhi98pp

Atom	Orbital	r_{cut}(Bohr)	Atom	Orbital	r_{cut}(Bohr)
Li		core corrected	Na		core corrected
	2s	2.181868		3s	2.701187
	2p	2.181868		3p	2.701187
	2d	2.464973		3d	2.978116
Si			Cl		
	3s	1.703918		3s	1.585300
	3p	1.878606		3p	1.585300
	3d	2.021277		3d	1.790998
Cu			Al		
	4s	2.079001		3s	1.7907575
	4p	2.292143		3p	1.9743480
	3d	2.079001		3d	2.1242906
C			Ga		
	2s	1.498153		4s	2.092576
	2p	1.498153		4p	2.251497
	3d	1.498153		3d	2.092576
	4f	1.498153		4f	2.092576
As			F		
	4s	1.965753		2s	1.338522
	4p	2.167285		2p	1.338522
	4d	2.448497		3d	1.338522
Rh			Pd		
	5s	2.465805		5s	2.471781
	5p	2.589120		5p	2.595395
	4d	2.348363		4d	2.354055
	4f	2.348363		4f	2.354055
Ge			Ag		
	4s	1.978319		2s	2.419190
	4p	2.181138		2p	2.602917
	4d	2.464148		2d	2.419190
	4f	2.464148			

Chapter 5

Performance of GGA's

Within this chapter we will focus on the reduction of the raw results mentioned in chapter 4. We will look at how well the PsP calculations measure up to the more accurate AE calculations for the target ground-state properties. We will be looking at the performance of the test set as a whole as well as each solid individually. Then, we will explore the effects of mixing the methods used to describe the valence and core electrons.

5.1 PsP Ground-State Properties Versus AE

The three ground-state properties that are the target for this research are lattice constant, bulk modulus, and cohesive energy. Detailed descriptions of these values and how they are obtained can be found in chapter 3. All of the raw results are reported in appendix B along with the experimental values reported in chapter 3.

In order for us to gauge how well a PsP calculation performed, all the following results will be reported in three formats: the mean relative error (in %),

$$\mathrm{MRE} = \frac{1}{n}\sum_{i=1}^{n} 100\frac{p_i^{calc} - p_i^{exp}}{p_i^{exp}} \tag{5.1}$$

the mean absolute relative error (in %),

$$\text{MARE} = \frac{1}{n}\sum_{i=1}^{n} 100 \left| \frac{p_i^{calc} - p_i^{exp}}{p_i^{exp}} \right| \tag{5.2}$$

and the spread (in %)

$$\text{Spread} = \max\left(100\frac{p_i^{calc}}{p_i^{exp}}\right) - \min\left(100\frac{p_i^{calc}}{p_i^{exp}}\right) \tag{5.3}$$

In all cases p_i^{calc} is the value of the ground-state property we calculated and p_i^{exp} is the experimental or AE value. The MRE will allow us to see how accurate, on average our results are. The MARE value will help determine the strength of the MRE value. If the MRE and MARE values are very close to each other then the results are consistently in the direction of the MRE. However, if the MRE and MARE are very different little can be said about the MRE result. The spread will pick up any outliers or give hints to the level of precision. Unless otherwise noted, these values will include all sixteen solids in the test set.

5.1.1 Lattice Constants

Before we can really see how well our PsP result can predict the ground-state properties, we must address the question posed at the beginning as to whether or not we can reproduce the AE results. To test this we have focused on the lattice constant value as we find it to be the most informative of the the three properties. We will be looking at the PsP results for three functionals LDA, PBE, and PBEsol as that is where we have AE data.

In figure 5.1 we have plotted the percent difference from AE results for the lattice constant. The AE values used to make this plot are an average of two AE data sets for each functional [35, 26, 36, 37]. This was done to create an average lattice constant one can expect from an AE calculation. This figure shows that our PsP

Table 5.1: The table has the MRE, MARE, and spread in lattice constant for our LDA, PBE, and PBEsol PsP data sets compared with average AE results.

Functional	MRE %	MARE %	Spread %
LDA	-0.157	0.511	2.671
PBE	-0.003	0.780	3.427
PBEsol	0.040	0.783	3.346

results only vary from 0.11% to 1.89% from the average AE results. Because the zero of the plot represents the PsP and AE results having the same lattice value, any point above means a PsP result with a larger lattice constant and any point below means a PsP with a smaller lattice constant. This shows that our PsP results tend to under-bind, have larger lattice constant, more for solids with heavier elements in them and over-bind, have a smaller lattice constant, for the solids made of lighter elements.

If we look at the MRE, MARE and Spread of our results we can gain some information about how the PsP calculations for each functional performs compared to AE calculations. In table 5.1 we can see that the more accurate PsP, on average, is the PsP treatment of PBE with a MRE of -0.003%, however the PsP treatment of LDA is more precise with a Spread of only 2.671%. However, in all causes the MARE and MRE values do not match up so little can be gained from this analysis. What can be said is that our PsP results predict similar lattice results to AE but lose out on the precision of the results.

We can now start to compare our PsP results with experiment starting with the LDA functional. Figure 5.2 has the percent difference from experiment for each solid along with the percent difference from experiment for two AE data sets and one PsP data set [34]. As can be seen, our results follow the AE results with the added errors

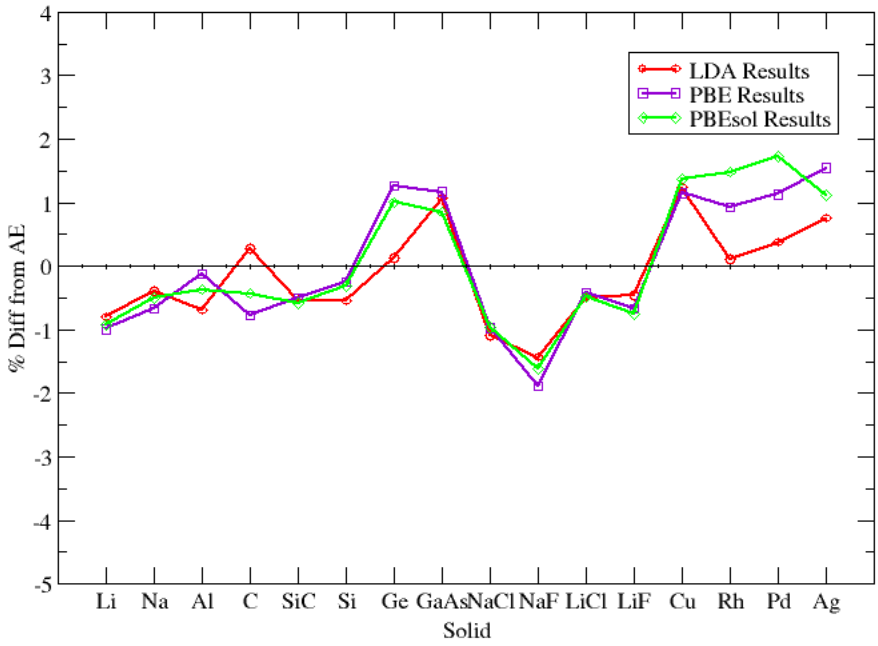

Figure 5.1: Here we have the percent difference from AE theory for the three functionals we have AE data for: LDA, PBE, and PBEsol. We can see that our PsP calculations only deviate from the AE by a max of 1.9%.

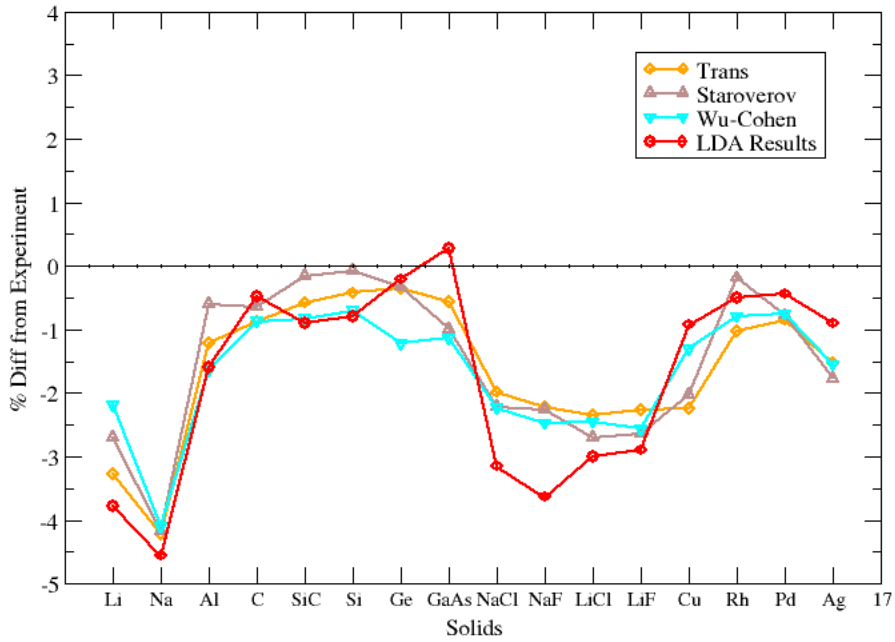

Figure 5.2: The percent difference from experiment is plotted for our LDA lattice constant results along with other AE calculations.

from the PsP as noted above. Also, both our PsP results and the AE results share a common trend of having a net over-binding in the systems, causing a smaller lattice constant. GaAs for our data set is the only exception to this trend. This deviation can be explained by the large under-binding caused by the PsP for GaAs seen in figure 5.1.

Next, in figure 5.3 we look at our PsP treatment of PBE lattice results; also plotted with the two AE results. The trend we saw before with LDA, has now flipped for the majority of the systems to under-binding. Besides Li and Na which over-bind for all data sets, the only one that doesn't share the trend is C for our data. We can also attribute this to our PsP causing additional errors compared to its AE counterparts.

Finally in figure 5.4 our PsP treatment of PBEsol lattice constant results are

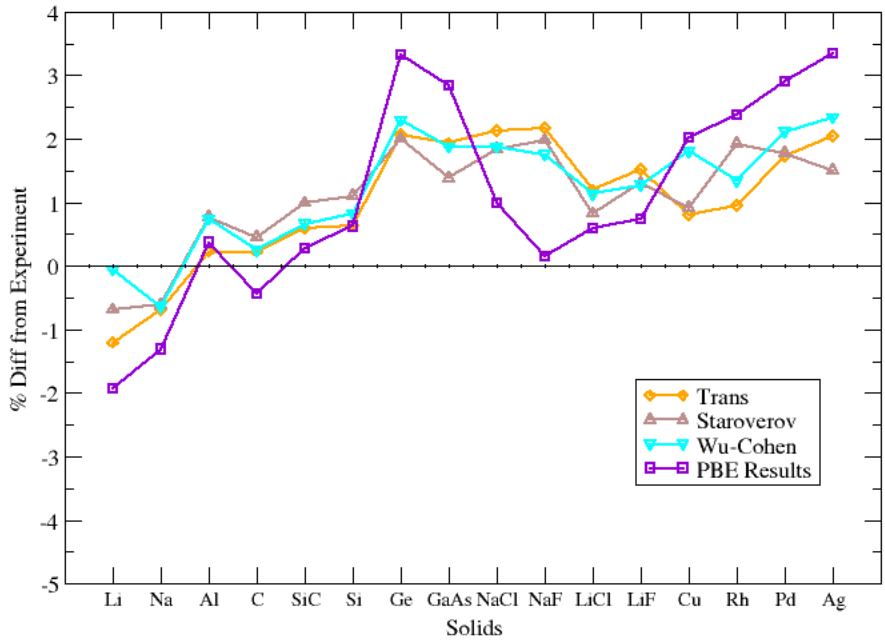

Figure 5.3: The percent difference from experiment is plotted for our PBE lattice constant results along with other AE calculations.

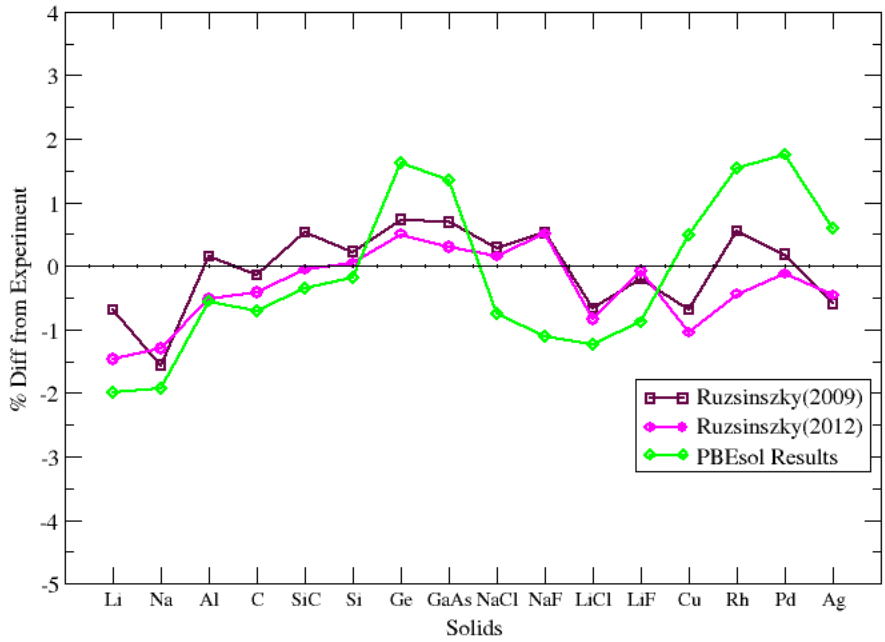

Figure 5.4: The percent difference from experiment is plotted for our PBEsol lattice constant results along with other AE calculations.

plotted along with data from two different AE studies [36, 37]. Where as before LDA would over-bind and PBE would under-bind, we find PBEsol falls some where in between the two. This is to be expected as the PBEsol gradient correction is about half that of the PBE. We can also see more clearly the effect of the additional errors of the PsP compared to the AE, specifically for the ionic compounds and transition metals.

5.1.2 Bulk Moduli

As with the lattice constant, we have plotted the percent difference from experiment in bulk modulus for each solid. Also along with those results are bulk modulus values from AE calculations previously mentioned in the above section. The first plot (figure

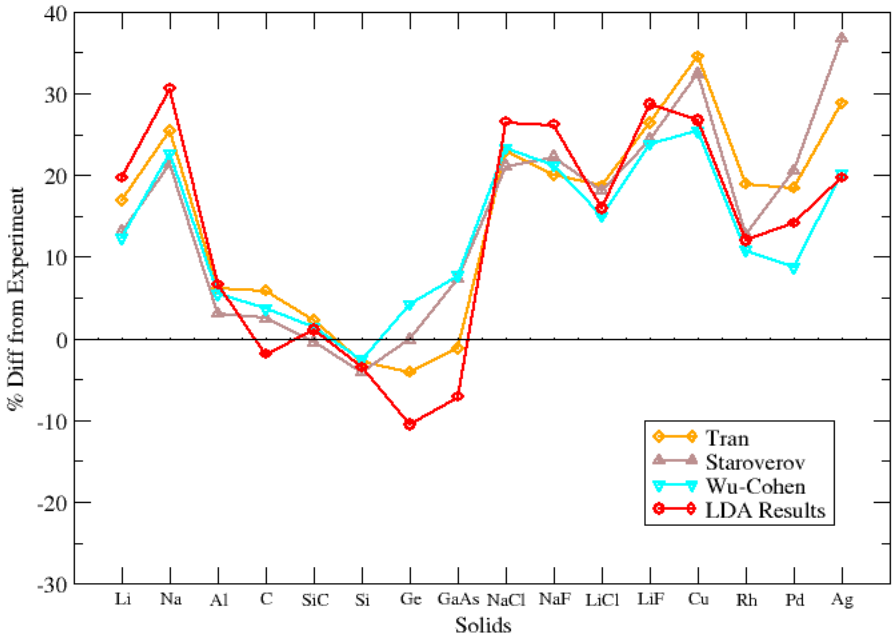

Figure 5.5: The percent difference from experiment is plotted for our LDA bulk modulus results along with other AE calculations.

5.5) has the results for the PsP treatment of LDA functional. As seen before, our results trend with the AE results. Also, on average, a LDA calculation estimates a system that is 'too hard' compared to experiment.

Next in figure 5.6 we have the PsP treatment of PBE functional bulk modulus results plotted. Similar as before, it trends with AE but in this case the data sets are tighter then the LDA results. We can also see that all the sets tend to predict the systems as 'too soft' compared to experiment.

Finally in figure 5.7 the PsP treatment of PBEsol functional bulk modulus results are plotted. Unfortunately, we currently have only one set of AE results to compare too. This makes it hard to say much about how well we compare to an AE calculations. At best we can see the PsP results trend with AE and the bulk modulus values fall

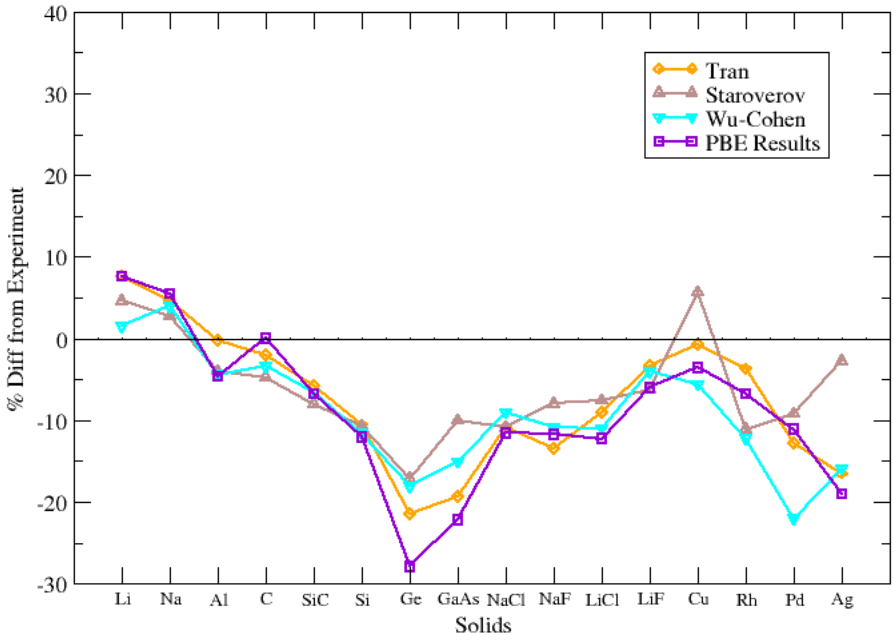

Figure 5.6: The percent difference from experiment is plotted for our PBE bulk modulus results along with other AE calculations.

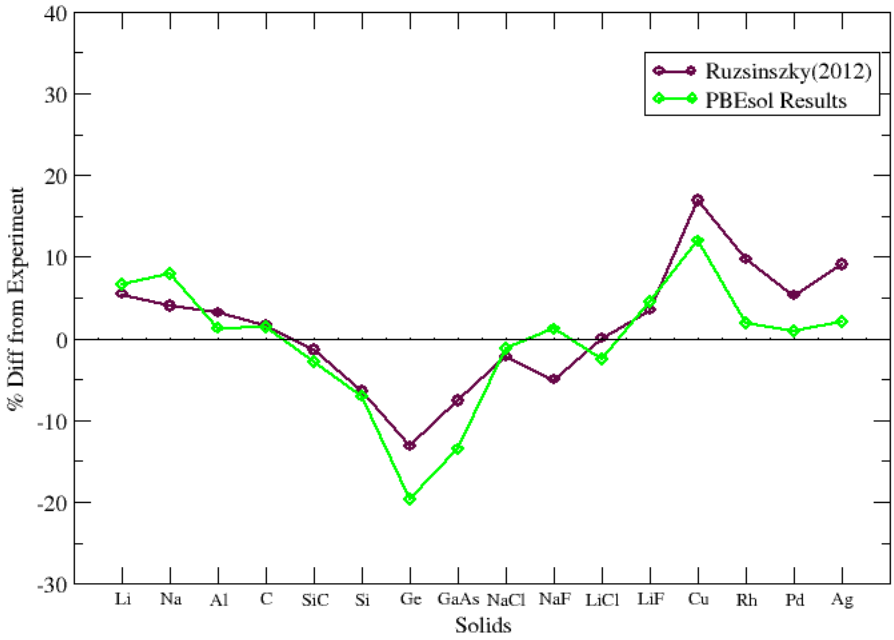

Figure 5.7: The percent difference from experiment is plotted for our PBEsol bulk modulus results along with other AE calculations.

between those of PBE and LDA.

5.1.3 Cohesive Energies

We now come to the final target property: cohesive energy. Out of all the data sets we had collected, only two of them had cohesive energy results and one of them was a PsP calculation. This makes it difficult to draw any hard conclusions about our results, however, they are presented still the same. In figure 5.8 we can see that our results trend with 'Wu-Cohen' which is the other PsP calculation. When we look at the AE results we can see wild variations. The most notable differences are for GaAs, LiF, and LiCl. Without additional data sets it is hard to say whether these differences are caused by the use of PsP's or the 'Ruzsinszky' AE data set being incorrect.

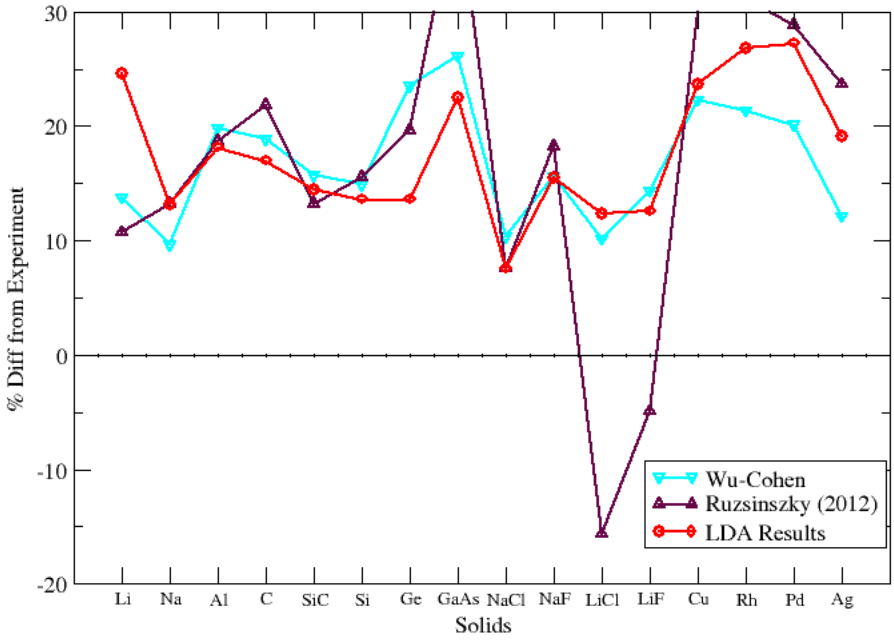

Figure 5.8: The percent difference from experiment is plotted for our LDA cohesive energy results along with other AE calculations.

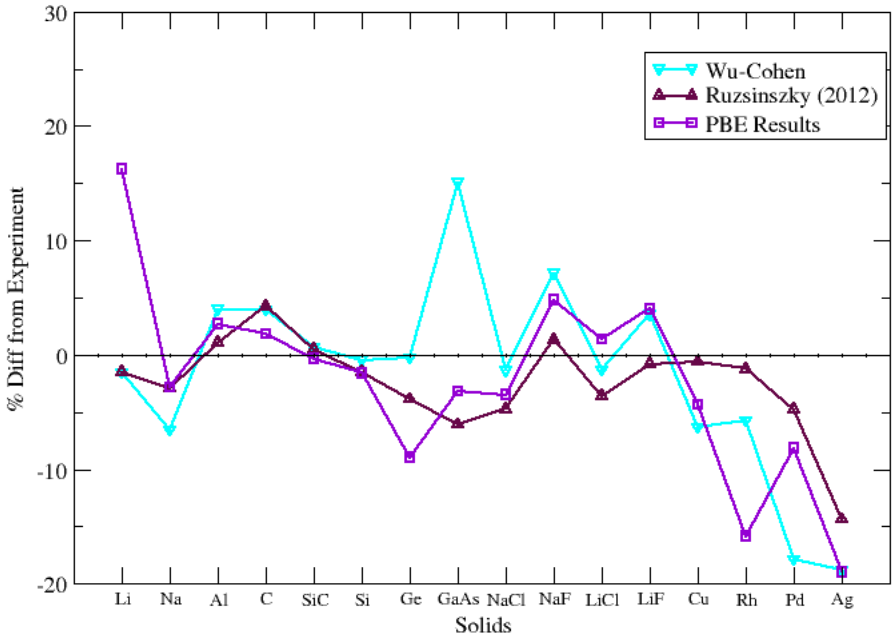

Figure 5.9: The percent difference from experiment is plotted for our PBE cohesive energy results along with other AE calculations.

The PsP treatment of PBE and PBEsol results in figure 5.9 and 5.10 are also plotted. The AE results in these cases are less erratic and our values do trend with them. Once again it is hard to say much more beyond that without additional data.

5.2 Functional Performance with PsP's

With the analysis from above showing that our results trend with AE results with some noted differences, we can examine how the functionals are performing within the PsP environment. To start we have plotted the lattice constant results for all the functionals we tested in figure 5.11. Not only have we plotted the previously examined LDA, PBE, and PBEsol functionals, we have also included our results with mixed functionals. The mixed functionals have a PsP describing the core with one

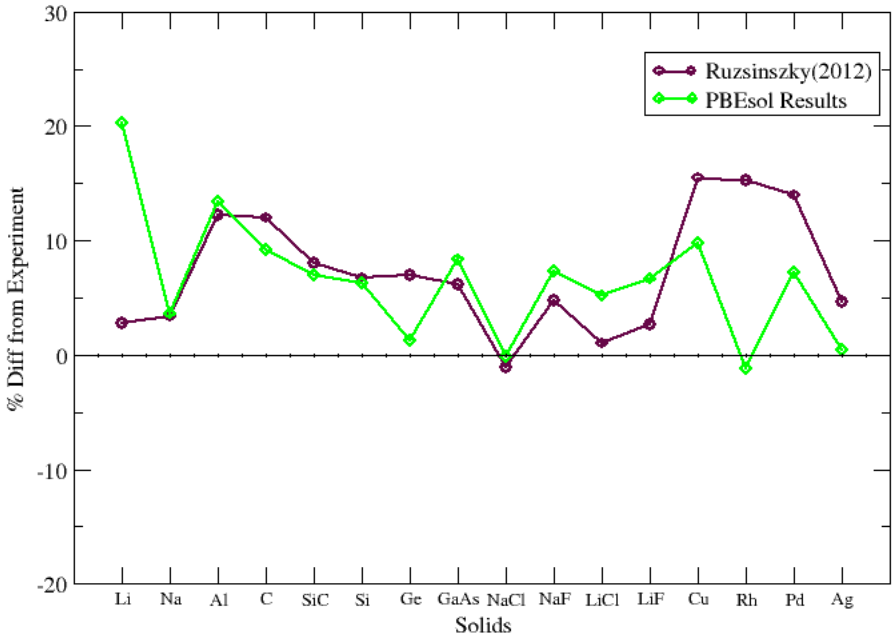

Figure 5.10: The percent difference from experiment is plotted for our PBEsol cohesive energy results along with other AE calculations.

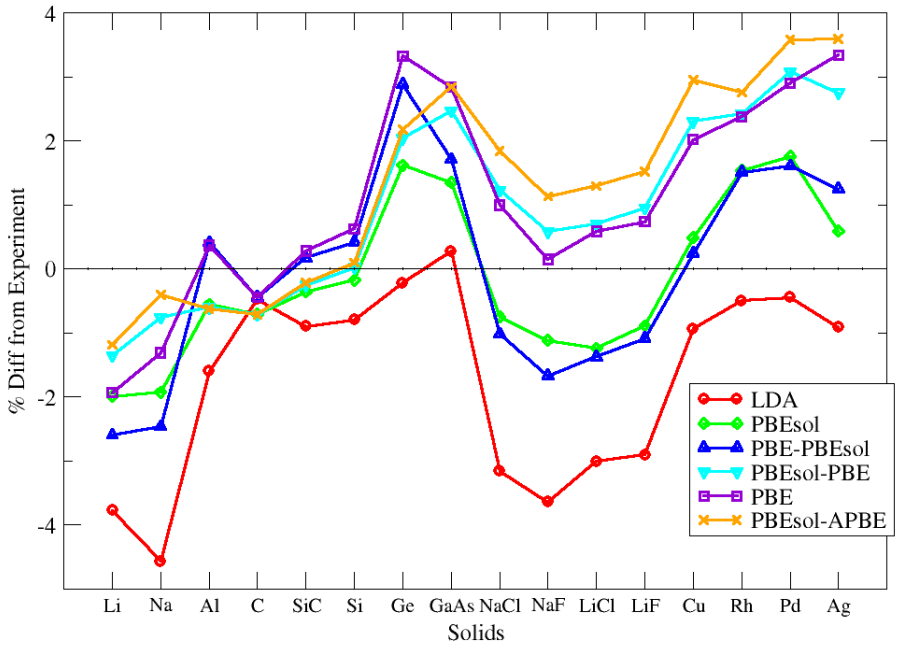

Figure 5.11: The percent different from experiment in lattice constant is plotted for each solid in our test. This plot has all our functionals test showing the differences between the functionals and the use of mixing methods

functional and a DFT calculation describing the valence with another functional. For example PBE-PBEsol is the core described using PBE and the valence with PBEsol. We have three mixed functionals that we tested: PBEsol-PBE, PBE-PBEsol, and PBEsol-APBE.

The first thing to notice is that all our data sets have similar trends, only shifted up or down. This is a wonderful result as it shows we have self-consistent results and the major effects we are seeing on these plots are from the functionals used. The second thing to note is the trend from over-binding to under-binding as the strength of the gradient correction is increased. The LDA which has zero gradient correction ($\mu = 0$) over-binds the most. PBE, which has a strong gradient correction ($\mu = 0.21951$)

under-binds. PBEsol, which has a weaker gradient correction ($\mu = 0.12346$) falls in between LDA and PBE. APBE with the strongest gradient correction ($\mu = 0.26037$) under-binds the most.

Looking at our mixed functionals we can see something interesting with regards to how the solids fall onto the plot. For the simple metals and semiconductors, the functionals that share the same core functional correlate more. On the other hand, for the ionic compounds and transition metals, the functionals that share valence functionals seem to correlate more. For example the 'PBE-PBEsol' data set follows the 'PBE' data set until NaCl then it shifts down to the'PBEsol' data set. This suggests that the simple metals and semiconductors are more effected by core effects.

The mixed functional 'PBEsol-APBE' needs some additional attention. Like noted above it too jumps between the functionals that compose it. It starts to trend with 'PBEsol-PBE' and 'PBEsol' then diverges off above 'PBE'. The data trending above 'PBE' is some what expected as APBE is a variant of PBE with a stronger gradient correction but it is closer then the difference between the PBE and PBEsol groups. To better understand what is happing with the APBE, a new data set would be needed that has both the valence and core described by APBE.

To measure the overall performance of each functional for lattice constant, the MRE, MARE, and spread for each is listed in table 5.2. The LDA result has the strongest MRE result as its MARE value is almost the same value. This means that all the LDA results are consistently over-bound. As the MRE value grows smaller (the results get closer to experiment on average) the MARE value deviates more. This means that as the results improve in accuracy on average they decrease in precision. The set with the best MRE value of -0.028% is the PBE-PBEsol but the MARE value is not on the same order so the results are erratic. The functional that is both most accurate and precise is PBEsol for the lattice constant. This result makes sense

Table 5.2: The table has the MRE, MARE, and spread in lattice constant for our test set with each functional tested. The most precise is the PBEsol where the most accurate is the mixed functional PBE-PBEsol.

Functional	MRE %	MARE %	Spread %
LDA	-1.721	1.756	4.846
PBEsol	-0.148	1.065	3.745
PBE-PBEsol	-0.028	1.304	5.482
PBEsol-PBE	0.931	1.388	4.427
PBE	1.055	1.515	5.275
PBEsol-APBE	1.291	1.684	4.777

as the PBEsol functional was designed to improve results like lattice constant for solids.

We now move on to the bulk modulus values plotted in figure 5.12. Similar to the lattice plot, the data sets trend with each other and we can see the grouping as we did before. To get a better feel for the bulk modulus results we look at the overall performance.

The MRE, MARE, and the spread in bulk modulus for each XC functional are listed in table 5.3. The set with the best MRE is the PBEsol with a value of -0.438% but does not match with its MARE value so the results is not very strong. The one with the best MRE and MARE match is PBEsol-APBE showing that the results are consistently under the expected.

Finally we come to the cohesive energy results in figure 5.13. Like the other two plots above, the data sets trend with each other. One major difference in this plot is the way the sets group. Noted above, we saw the mixed functionals switch between the two functionals that composed them. For cohesive energy that is not the case and they group by the functional used to describe their valence electrons. This shows that the ground-state property of cohesive energy is dominated by the valence interactions.

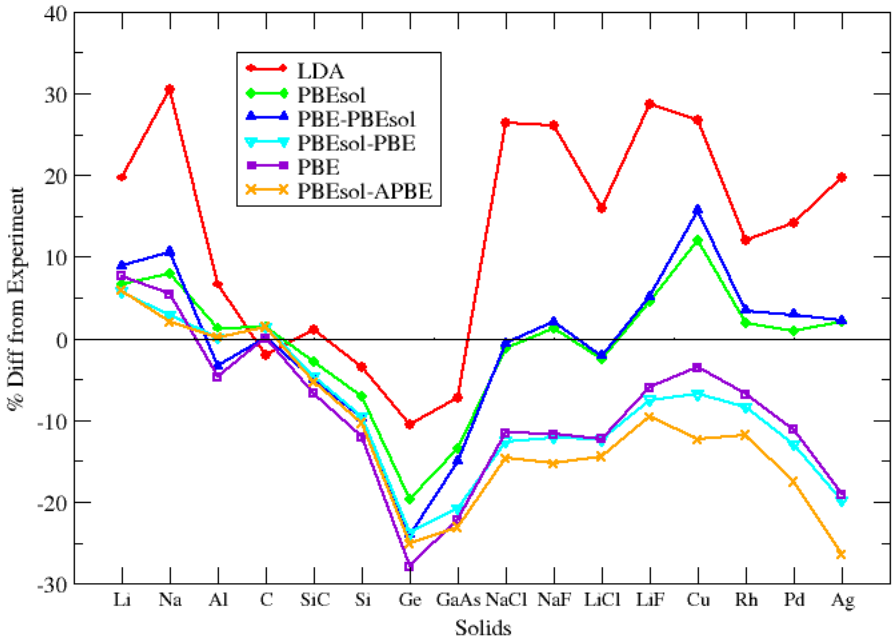

Figure 5.12: The percent different from experiment in bulk modulus is plotted for each solid in our test. This plot has all our functionals test showing the differences between the functionals and the use of mixing methods

Table 5.3: The table has the MRE, MARE, and spread in bulk modulus for our test set with each functional tested. The most precise is the mixed functional PBEsol-PBE where the most accurate is PBEsol.

Functional	MRE %	MARE %	Spread %
LDA	12.761	15.673	41.116
PBEsol	-0.438	5.413	31.632
PBE-PBEsol	-0.557	6.919	39.701
PBEsol-PBE	-8.826	10.090	29.540
PBE	-8.906	10.546	35.524
PBEsol-APBE	-11.042	12.220	32.293

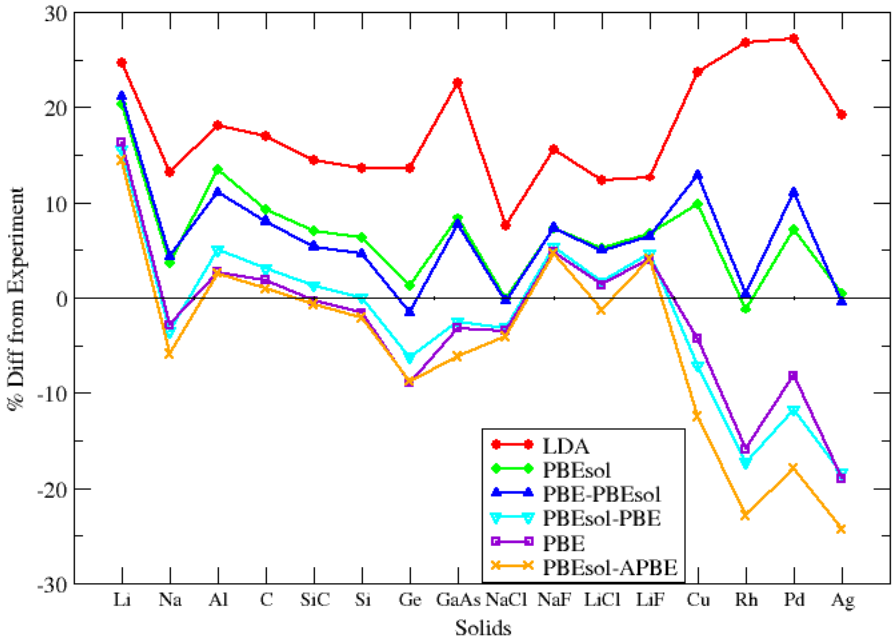

Figure 5.13: The percent different from experiment in cohesive energy is plotted for each solid in our test. This plot has all our functionals test showing the differences between the functionals and the use of mixing methods

Table 5.4: The table has the MRE, MARE, and spread in cohesive energy for our test set with each functional tested. The most precise is LDA where the most accurate is the mixed functional PBEsol-PBE.

Functional	MRE %	MARE %	Spread %
LDA	17.606	17.606	19.703
PBEsol	6.541	6.709	21.503
PBE-PBEsol	6.421	6.712	22.644
PBEsol-PBE	-2.100	6.660	33.966
PBE	-2.290	6.167	35.220
PBEsol-APBE	-4.992	8.318	38.697

The overall performance of the cohesive energy results are listed in table 5.4. The table shows that the strongest MRE value is the LDA results with a exact match in the MARE. This means all the LDA results are consistently too large. Both PBEsol and PBE-PBEsol have MRE and MARE values that are similar that allow us to say that the results are truly improving.

5.2.1 Solid Type Performance

Above we have looked at how each solid compares with experiment and how a data set as a whole performs, but we are now going to look at the performance of solid types. In the beginning of this thesis it was detailed that the solids selected fell into one of four types: simple metals, semiconductors, ionic compounds, or transition metals. It can then be assumed that solids of the same type will behave in a similar manner depending on the functional used. For this reason we can get a gauge for how well a functional in the PsP environment performs per solid type.

In figure 5.14 the MRE in lattice constant for a solid type is plotted for each functional tested along with the overall MRE for that functional type as listed in the previous tables. First, looking at the overall trend of the data, each functional has a

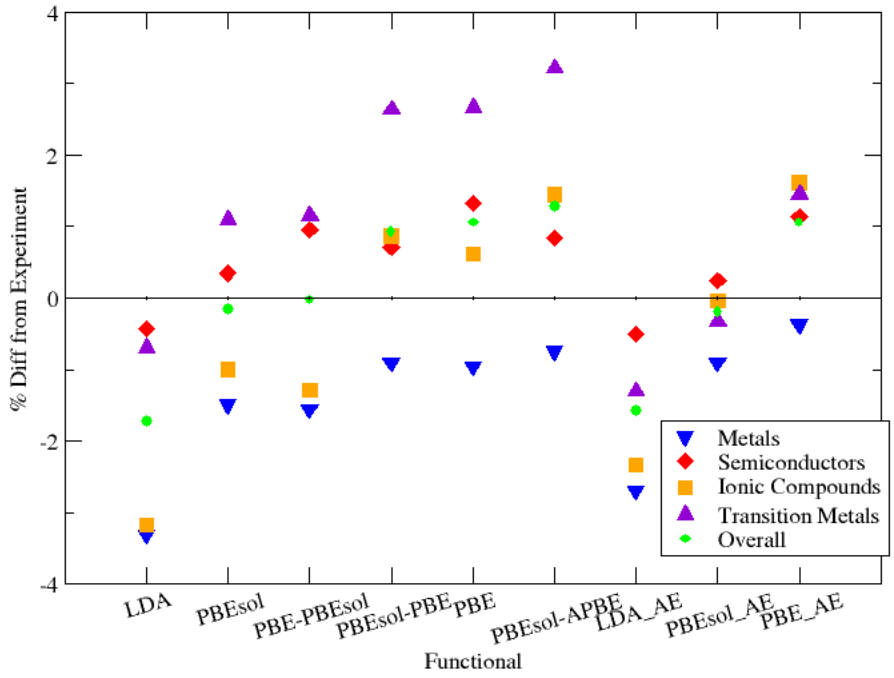

Figure 5.14: For each solid type within the test set its MRE in lattice constant is plotted. The 'overall' data set shows where the MRE value falls for each functional

similar spread across the different solid types just shifting its average upward. This upward trend also follows with the increase in gradient correction from one functional to the next.

Next, looking at where the solid types fall we can see that for every data set the simple metals are always over-bound. On the other hand (except for LDA) the semiconductors and transition metals are always under-bound. It is this spread between simple metals and transition metals that dominates where the overall MRE falls. The smallest of these spreads is seen for PBEsol and PBE-PBEsol. As PBEsol is designed to perform better for solids then PBE, this result is expected.

Noted above, we saw that the ionic compounds and transition metals appeared to be more effected by the functional used to describe the valence. This plot helps to confirm that for the transition metals. The 'PBEsol' and 'PBE-PBEsol' transition metal values fall right in line with one another. The same is true for the transition metal data points for 'PBEsol-PBE' and 'PBE'. The trend is less apparent for the ionic compounds but it is still noticeable. Surprisingly it appears that the simple metals also follow this trend. Where as before it appeared that they where effected by the functional describing the core, here they are correlated to the functional describing the valence.

There is one more interesting thing to note; the MRE values for PBEsol and PBE-PBEsol reported in table 5.2 are only good by chance. The spread in the solid types fall in such a way that the overall average just so happens to land very close to the experimental average.

Chapter 6

Discussion and Conclusions

Here we bring together the major results of this research. We will start off with noted limitations of PsP's found during our time creating our own. Then we will tackle the questions posed at the very beginning of this thesis. We end with a benchmark of what to expect when using GGA's in PsP environments.

6.1 Pseudopotential Limitations

PsP's are designed to leave only the chemical active valence electrons for calculations by removing the core electrons. This is done under the condition that the pseudo-orbital of the PsP matches the real orbital at a set radius. One challenge of the PsP is determining what is considered valence and what is core along with what a 'good' radial cut-off value would be. As discussed in chapter 4, this challenge can be meet and the PsP can be generated from the AE calculation of the neutral free atom. These PsP's are then used within DFT calculations to produce needed ground-state properties. From this, we have noticed that our PsP's do not perform as well as what we have considered to be the most theoretically accurate PsP calculation.

Table 6.1: The lattice constant values for the four ionic compounds in our test set along with the results from the 'Wu-Cohen' data set are reported. The percent relative error between the two is also reported.

Solid	a_0^{PBE} bohr	$a_0^{Wu-Cohen}$ bohr	Relative Error %
NaCl	10.682	10.775	-0.87
NaF	8.726	8.866	-1.58
LiCl	9.709	9.762	-0.54
LiF	7.949	7.677	-0.53

The discrepancy was noticed when comparing our lattice constant results with the 'Wu-Cohen' PsP data set [34] (figure 4.4). Two solid types stood out the most: ionic compounds and transition metals. Through additional literature and PsP documentation searches we have come across two possible reasons as to why we see the poor performance.

6.1.1 Ionic Compounds

Table 6.1 shows the lattice constant values for our PsP results and the Wu-Cohen results with the PBE functional. The percent relative error is also reported. Except for NaF which has a percent relative error of 1.58%, all of the ionic compounds have an error of less then 1%. A difference of 1% is approximately 0.1 bohr in lattice constant. As the goal was to match 'Wu-Cohen' as closely as possible, in order to make the effects of PsP's as small as possible it became important to characterize what could be causing this difference.

We speculate that the reason for the ionic compounds (and ultimately any diatomic system) performing poorly is an effect known as core polarization. Because PsP's are built from the free neutral AE calculations of atoms, the core that is replaced by the PsP is under no external effects from other atoms. Once an atom

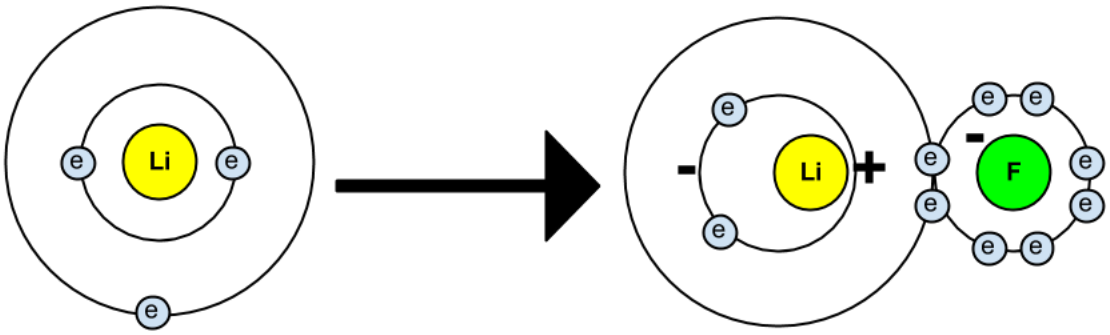

Figure 6.1: An exaggerated depiction of the core polarization in LiF

described with a PsP is placed in an environment with other charges, the valence electrons will adjust whereas the core will remain frozen. In actuality, the core of a real atom would respond to the external charges as well. In most situations the change of the core is so small that a PsP will still perform well. However, if the response of the real core to the external potential is large enough, the atom described with a PsP will not account for this change. This results in the difference between the real atom and the PsP atom becoming more apparent. For example take LiF; the Li gives up an electron to F so it can fill its outer shell. This causes the F to be negatively charged and attract the now positively charged Li: classic ionic bond. The Li still has another band of electrons though, and these electrons are repelled by the negatively charged F causing there probabilities to shift away from the bond region. This causes less screening of the Li nucleus from the negative F drawing it closer in, polarizing the Li atom (figure 6.1).

6.1.2 Transition Metals

The differences between our transition metal lattice constants and those of Wu-Cohen are on the order of those seen with the ionic compounds. The interesting results is

how well the ABINIT library PsP's seem to match Wu-Cohen where ours do not. This led us to investigate into what the ABINIT PsP's had done differently in order to agree with the Wu-Cohen results. We found that like our transitional metals they all had an empty p-state, except they had artificially raised the eigenvalue of that state causing it to act as though it was unbound. This brings forth the question as to why they would need to treat the empty p-state in this way.

P-states normally have a larger spatial volume than s- and d-states. It is because of this that when a p-state forms a bond, the resulting system is larger than if an s- or a d-bond would have formed. In the case of solids, this would translate to a larger lattice constant value. With this idea in mind, we know that our transition metal results have larger lattice constant values than those of ABINIT or Wu-Cohen. This draws us to the conclusion that p-bonds could be forming within our system instead of s- or d-bonds which could decrease the lattice constant.

We speculate, therefore; that the reason ABINIT is treating the empty p-states as unbound is to lower the p-state's potential for bonding within their systems. In doing so, it would cause s- and d-bonds to dominate resulting in a smaller lattice constants. This then allows the ABINIT lattice constant results to match better with the Wu-Cohen results whereas our results are too large. APE, however, does not allow for this kind of adjustment to the eigenvalues so we are unable to perform the same trick as ABINIT.

6.1.3 Conclusions

With this information presented regarding PsP's the only remaining question is: does one use a PsP from a library or make their own. If the goal is to test an aspect of DFT then avoid pre-made PsP's as we have done here. The reason being, you do not

know the motivation behind that PsP. It could have been built to provide values very close to experiment, or was designed to work well in molecular systems and not solids. This means that the PsP you could be retrieving from a library may hide effects of DFT that you may be looking for, or worse produce a false result.

There are also the limitations of PsP discussed above. PsP's are unable to reproduce the effects of core polarization causing poor results for diatomic systems. There is also the issue of transition metals and what appears to be unwanted binding of the p-states. These affects may or may not have been treated for in a PsP from a library. It is concluded better to generate your own and, if one must use a PsP from a library, use it with caution.

6.2 GGA Performance

The first question we posed in the beginning of this thesis was whether or not a PsP calculation can still provide the accuracy of an AE calculation. We explored this question in chapter 5 by looking at how well our PsP results stacked up to a set of AE results. First, we saw that our PsP's could reproduce the common trends seen for the functionals tested. The lattice constant results for example over-bound for LDA, under-bound for PBE, and PBEsol split the difference. We did note, however, that solids made up of heavier elements tended to under-bind compared to AE averages. The majority of these heavier elements are transition metals which we have already noted as being treated poorly by our PsP's. In fact, we have seen that all our transition metal results under-bind more then other PsP results. Those made up of lighter elements, in contrast, tended to over-bind compared to AE averages. The majority of these systems are the ones we noted above for having issues with reproducing the effects of core polarization. Even with these differences the largest

discrepancy from the AE averages in lattice constant was only 1.9%.

The second question we set out to answer was what was the affect of using one functional to describe the core electrons and another to describe the valence. The plot that really shows the affect best is 5.11. The lattice results for the mixed data sets flip-flop between the results of the functional that compose them. What this means is the description of the XC is changing based on what kind of system the calculation is done in. Ultimately, if the core and valence are described using different methods it is possible to have better results **on average**, however, this does not mean that the result will be any more precise.

Knowing that PsP calculations can be used instead of AE calculations, noting the loses in accuracy as stated above, we have a benchmark for how other GGA's will perform with PsP's. We know to expect more under-binding with stronger gradient corrections. We know that the mean relative error for a GGA's performance will be dominated by the performance of the simple and transition metals. We can expect poor accuracy for transition metals and systems with large core polarization. Finally we know that the results are more predictable if the core and valence are described using the same functional even though the results may not be as accurate.

Thinking back on the research done, there are some things that could have affected the results. One such aspect could be the convergence parameters of the solids and free atoms used in ABINIT. We converged the energy values such that the difference between iterations was less then 0.001 Hartree. This could be pushed even further to insure that the convergence is not an issue. Another piece that could be adding bias to the results is the number of solids tested. We studied five semiconductors and four transition metals compared to three simple metals. Mentioned in chapter 5, the simple metals and transition metals dominated the location of the MRE for a functional. If we had more simple metals within the data set this may no longer be

the case.

6.2.1 Future Considerations

This study focused on a total of 16 solids from different types of materials. To improve our understanding on the overall performance and the solid type performance, the addition of more solids to the test set is recommended. The most lacking is simple metals with only three represented in the test set here.

In addition to the inclusion of more solids, another study with the APBE functional would help shed more light on its behaviour. Within this thesis, we only focused on the mixed functional PBEsol-APBE, but did not do a full APBE data run. The expected result, based on APBE's foundation in atomic systems, would be poor performance for lattice constant and bulk modulus but an improved performance for cohesive energy.

More investigation into the PsP limitations noted here is also needed. The confirmation and detailed description of the p-state bonding effect in transition metals may help fix the issues. Also, a study into measuring the effect of core polarization would greatly improve the results for all diatomic systems.

Appendix A

List of Acronyms

ABINIT Open-source Density Functional Theory coding package

AE All Electron

APBE varient of PBE designed from atomic data

APE Atomic Psuedopotential Engine

BZ Brillouin Zone

DFT Density Functional Theory

DNA Deoxyribonucleic acid

fhi98PP Pseudopotential generating code package

GGA Generalized Gradiant Approximation

GTO Gaussian-Type Orbital

HEG Homogeneous Electron Gas

KS Khon-Sham

LDA Local Density Approximation

NNIN National Nanotechnology Infrastructure Network

PBE Perdew-Burke-Ernzerhof

PBEsol varient of PBE to improve solid preformence

PsP Pseudopotential

XC Exchange-Correlation

ZPE Zero Point Energy

Appendix B

Raw DFT results with PsP's

Here we have listed all the raw ground-state property results detailed in chapter 3 with the PsP's we generated (ch. 4). Each table has the results for three primary XC functionals (LDA, PBE, and PBEsol) along with the mixed functionals (PBE-PBEsol, PBEsol-PBE, and PBEsol-APBE). Table B.1 has all the lattice constant results, table B.2 has all the bulk modulus results, and table B.3 has all the cohesive energy results.

Table B.1: The raw lattice constant values for the whole test set. All values are in bohr. Note: superscripts like PBE-PBEsol should be read as PBE core with PBEsol valence.

Solid	a_0^{LDA}	a_0^{PBEsol}	$a_0^{PBE-PBEsol}$	$a_0^{PBEsol-PBE}$	a_0^{PBE}	$a_0^{PBEsol-APBE}$
Li	6.325	6.442	6.402	6.484	6.446	6.495
Na	7.622	7.833	7.790	7.927	7.882	7.954
Al	7.500	7.580	7.653	7.576	7.650	7.574
C	6.711	6.695	6.713	6.695	6.713	6.695
SiC	8.164	8.209	8.252	8.217	8.261	8.220
Si	10.183	10.246	10.308	10.267	10.329	10.275
Ge	10.661	10.858	10.992	10.902	11.040	10.917
GaAs	10.706	10.821	10.860	10.940	10.980	10.980
NaCl	10.242	10.497	10.469	10.707	10.682	10.771
NaF	8.395	8.616	8.567	8.763	8.726	8.811
LiCl	9.362	9.533	9.519	9.719	9.709	9.777
LiF	7.360	7.513	7.498	7.652	7.636	7.696
Cu	6.748	6.844	6.827	6.968	6.949	7.012
Rh	7.144	7.290	7.288	7.354	7.350	7.377
Pd	7.304	7.465	7.455	7.562	7.550	7.599
Ag	7.622	7.737	7.788	7.904	7.949	7.968

Table B.2: The raw bulk modulus values for the whole test set. All values are in $10^{11}\frac{N}{m^2}$. Note: superscripts like PBE-PBEsol should be read as PBE core with PBEsol valence.

Solid	B_0^{LDA}	B_0^{PBEsol}	$B_0^{PBE-PBEsol}$	$B_0^{PBEsol-PBE}$	B_0^{PBE}	$B_0^{PBEsol-APBE}$
Li	0.156	0.139	0.142	0.137	0.140	0.138
Na	0.098	0.081	0.083	0.077	0.079	0.076
Al	0.846	0.804	0.767	0.795	0.757	0.795
C	4.342	4.493	4.431	4.493	4.431	4.493
SiC	2.273	2.186	2.139	2.145	2.098	2.130
Si	0.957	0.922	0.896	0.898	0.872	0.889
Ge	0.678	0.609	0.576	0.577	0.547	0.568
GaAs	0.702	0.654	0.642	0.599	0.588	0.581
NaCl	0.336	0.263	0.265	0.232	0.235	0.227
NaF	0.648	0.520	0.524	0.452	0.454	0.435
LiCl	0.411	0.345	0.346	0.310	0.311	0.303
LiF	0.898	0.729	0.734	0.646	0.656	0.631
Cu	1.799	1.590	1.643	1.324	1.369	1.244
Rh	3.013	2.740	2.781	2.465	2.507	2.372
Pd	2.225	1.968	2.007	1.698	1.733	1.608
Ag	1.304	1.112	1.114	0.874	0.883	0.802

Table B.3: The raw cohesive energy values for the whole test set. All values are in hartree. Note: superscripts like PBE-PBEsol should be read as PBE core with PBEsol valence.

Solid	E_{coh}^{LDA}	E_{coh}^{PBEsol}	$E_{coh}^{PBE-PBEsol}$	$E_{coh}^{PBEsol-PBE}$	E_{coh}^{PBE}	$E_{coh}^{PBEsol-APBE}$
Li	0.075	0.072	0.073	0.069	0.070	0.069
Na	0.046	0.042	0.043	0.039	0.040	0.038
Al	0.148	0.142	0.139	0.131	0.128	0.128
C	0.636	0.594	0.587	0.560	0.554	0.549
SiC	0.536	0.501	0.493	0.474	0.467	0.465
Si	0.386	0.362	0.356	0.340	0.335	0.333
Ge	0.323	0.288	0.280	0.267	0.259	0.259
GaAs	0.302	0.267	0.265	0.240	0.239	0.231
NaCl	0.257	0.239	0.238	0.232	0.231	0.229
NaF	0.321	0.298	0.298	0.292	0.291	0.291
LiCl	0.288	0.269	0.269	0.260	0.260	0.253
LiF	0.360	0.342	0.341	0.335	0.333	0.333
Cu	0.159	0.141	0.145	0.119	0.123	0.112
Rh	0.268	0.209	0.212	0.175	0.178	0.163
Pd	0.182	0.154	0.159	0.126	0.132	0.118

Appendix C

Atomic Orbitals in ABINIT

In every case of isolated atomic systems, ABINIT requires the addition of an empty band for convergence. The reason behind this is how ABINIT searches for the minimum energy of a system. It will explore the atomic orbitals looking for the minimal configuration. If there is not an empty orbital it will not know that it is in a minimum configuration. Therefore an empty band is requested by ABINIT to insure convergence. This would mean that for Al, the input for the ABINIT variable *occ* would be

```
occ  1  1  0  0
     1  0  0  0
```

This will provide the one filled s-state and mostly empty p-state giving an electron configuration of $3s^2 3p^1$ and empty states for convergence. It is important to note that when dealing with p- or d-states with more than one electron present, *occ* can be written in two different ways. In the case of Pd which has a full d-state, it can be input as such

```
occ  5  0
     5  0
```

This would provide the 5-up and 5-down d-state electrons plus one empty band for convergence. Upon inspection, however, this is not correct. Examining the orbitals reveals that only two d-orbitals are created when there should be 5 d and 1 s (Figure C.1).

ABINIT is stuffing all the electrons into one band, a d-state, and leaving one empty band, also a d-state. Because ABINIT does not worry about the Paulie Principal it allows this to happen. This greatly effects the resulting energies causing them to differ greatly from previous results. In order to maintain consistent treatment of all the systems *occ* should be input as

```
occ  1  1  1  1  1  0  0  0  0
     1  1  1  1  1  0  0  0  0
```

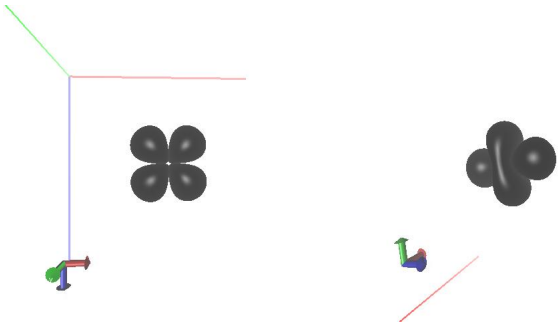

Figure C.1: Two atomic orbitals of Pd, both are d-states

Forcing two electrons per band and 9 total bands; 5 d-bands, 3 p-bands, and 1 s-band. This configuration now provides the correct number of bands(Figure C.2) and electrons per band along with empty bands.

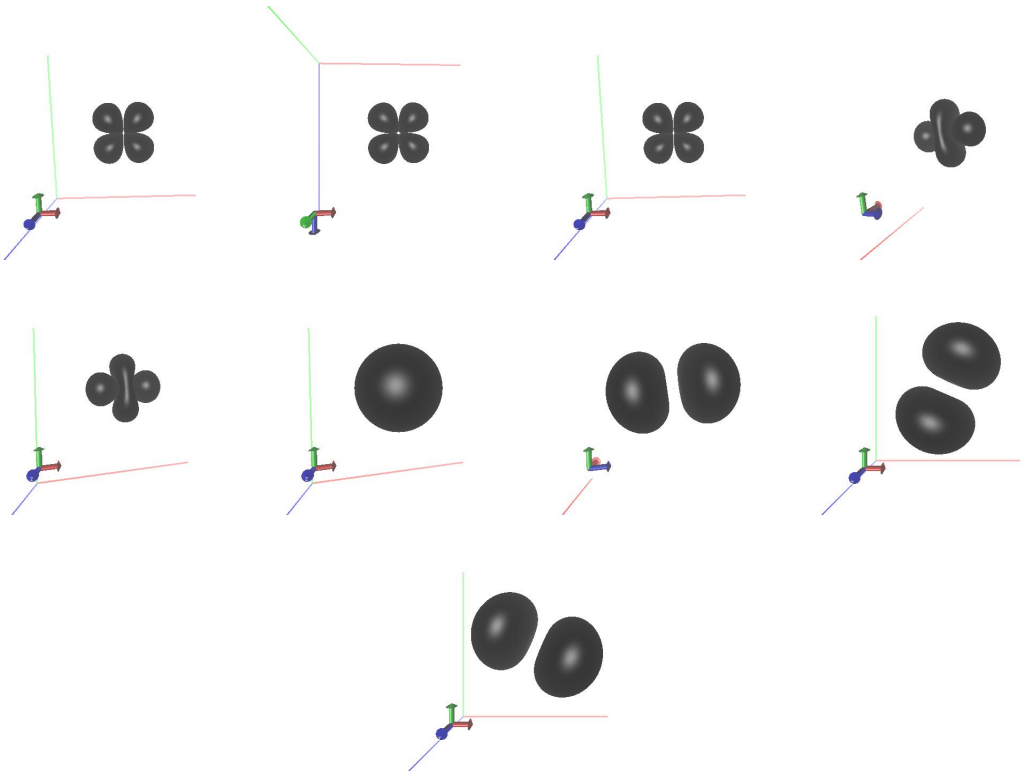

Figure C.2: Atomic orbitals of Pd. From the upper left corner across: 5 d-states, 1 s-state, 3 p-states

Bibliography

[1] P. Hohenberg and W. Kohn. *Inhomogeneous electron gas. Physical Review B* **139**, 864 (1964).

[2] W. Kohn and L. J. Sham. *Self-consistent equations including exchange and correlation effects. Physical Review* **140**, A1133 (1965).

[3] Xifeng Li, Zhongli Cai, and Michael D. Sevilla. *Investigation of proton transfer within dna base pair anion and cation radicals by density functional theory. J. Phys. Chem. B* **105**, 10115 (2001).

[4] Amitesh Maiti1, Alexei Svizhenko2, and M. P. Anantram. *Electronic transport through carbon nanotubes: Effects of structural deformation and tube chirality. Phys. Rev. Lett. B* **88**, 126805 (2002).

[5] Miguel A. L. Marques, Micael J. T. Oliveira, and Tobias Burnus. *Libxc: a library of exchange and correlation functionals for density functional theory. Comput. Phys. Commun.* **183**, 2272 (2012).

[6] J.P. Perdew, K. Burke, and M. Ernzerhof. *Generalized gradient approximation made simple. Phys. Rev. Lett.* **77**, 3865 (1996).

[7] J.P. Perdew, A. Ruzsinszky, G. I. Csonka, O. A. Vydrov, G. E. Scuseria, L. A. Constantin, X. Zhou, and K. Burke. *Restoring the density-gradient expansion for exchange in solids and surfaces. Phys. Rev. Lett.* **100**, 136406 (2008).

[8] L. A. Constantin, E. Fabiano, S. Laricchia, and F. Della Sala. *Semiclassical neutral atom as reference system in density functional theory. Phys. Rev. Lett.* **106**, 186406 (2011).

[9] U. von Barth and C.D. Gelatt. *Physical Review B* **21**, 2222 (1980).

[10] M. Born and R. Oppenheimer. *Ann. Phys.* **389**, 457 (1927).

[11] Richard Martine. *Electronic Structure: Basic Theory and Practical Methods.* Cambridge University Press (2004).

[12] D.M. Ceperley and B. J. Adler. *Ground state of the electron gas by a stochastic method. Phys. Rev. Lett.* **45**, 566 (1980).

[13] J. P. Perdew and Alex Zunger. *Self-interaction correction to density-functional approximations for many-electron systems. Phys. Rev. B* **23**, 5048 (1981).

[14] E. H. Lieb and S. Oxford. *Improved lower bound on the indirect coulomb energy. Intnational Journal of Quantum Chemisty* **19**, 427 (1981).

[15] J. P. Perdew, K. Burke, and Y. Wang. *Generalized gradient approximation for the exchange-correlation hole of a many-electron system. Physical Review B* **54**, 16533 (1996).

[16] P. Elliot and K. Burke. *Can. J. Chem.* **87**, 1485 (2009).

[17] D. Lee et al. *Semiclassical neutral atom as reference system in density functional theory. J. Chem. Phys.* **130**, 034107 (2009).

[18] D.R. Hamann. *Physical Review B* **40**, 2980 (1989).

[19] G. P. Kerker. *J. Phys. C: Solid State Phys.* **13**, L189 (1980).

[20] D. Vanderbilt. *Phys. Rev. B* **41**, 7892 (1990).

[21] N. Troullier and J.L. Martins. *Physical Review B* **43**, 1993 (1991).

[22] X. Gonze, B. Amadon, P.-M. Anglade, J.-M. Beuken, P. Boulanger F. Bottin, F. Bruneval and' D. Caliste, R. Caracas, M. Cote, T. Deutsch, L. Genovese, Ph. Ghosez, M. Giantomassi, S. Goedecker, D.R. Hamann, P. Hermet, F. Jollet, G. Jomard, S. Leroux, M. Mancini, S. Mazevet, M.J.T. Oliveira, G. Onida, Y. Pouillon, T. Rangel, G.-M. Rignanese, D. Sangalli, R. Shaltaf, M. Torrent, M.J. Verstraete, G. Zerah, and J.W. Zwanziger. *Abinit : First-principles approach of materials and nanosystem properties. Computer Phys. Commun.* **180**, 2582 (2009).

[23] X. Gonze, G.-M. Rignanese, M. Verstraete, J.-M. Beuken, Y. Pouillon, R. Caracas, F. Jollet, M. Torrent, G. Zerah, M. Mikami, Ph. Ghosez, M. Veithen, J.-Y. Raty, V. Olevano, F. Bruneval, L. Reining, R. Godby, G. Onida, D.R. Hamann, and D.C. Allan. Zeit. Kristallogr. *A brief introduction to the abinit software package. Computer Phys. Commun.* **220**, 558 (2005).

[24] Charles Kittel. *Introduction to Solid State Physics.* John Wiley & Sons (2005).

[25] H. J. Monkhorst and J. D. Pack. *Phys. Rev. B* **13**, 5188 (1976).

[26] Viktor N. Staroverov, Gustavo E. Scuseria, Jianmin Tao, and John P. Perdew. *Tests of a ladder of density functionals for the bulk solids and surfaces. Physical Review B* **69**, 075102 (2004).

[27] M. W. Chase. *JANAF Thermochemical Tables*. American Institute of Physics for the National Bureau of Standards (1986).

[28] F. D. Murnaghan. *The compressibility of media under extreme pressures. Proceedings of the National Academy of Sciences* **30**, 244 (1944).

[29] Behman Farid and R. W. Godby. *Cohesive energies of crystals. Physical Review B* **43**, 4248 (1991).

[30] *National Nanotechnology Infrastructure Network* (2011). `http://www.nnin.org/`.

[31] M. Fuchs and M. Scheffler. *Ab initio pseudopotentials for electronic structure calculations of poly-atomic systems using density-functional theory. Comput. Phys. Commun.* **119**, 67 (1999).

[32] M. Oliveira and F. Nogueira. *Atomic Pseudopotential Engine* (2012). `http://www.tddft.org/programs/APE/node/9`.

[33] J. M. Soler, E. Artacho, J. D. Gale, A. Garca, J. Junquera, P. Ordejn, and D. Snchez-Portal. *The siesta method for ab-initio order-n materials simulation. Phys.: Condens. Matt* **14**, 2745 (2002).

[34] Zhigang Wu and R. E. Cohen. *More accurate generalized gradien approximation for solids. Physical Review B* **73**, 235116 (2006).

[35] Fabien Tran and et al. *Preformance on molecules, surfaces, and solids of the wu-cohen gga exchange-correlation energy functional. Phys. Rev. B* **75**, 115131 (2007).

[36] Adrienn Ruzsinszky and et al. *Regular gradient expansion for atoms, molecules and soilds. J. Chem Theory Comp.* **5**, 763 (2009).

[37] Adrienn Ruzsinszky and et al. *A meta-gga made free of the order of limits anomaly. J. Chem Theory Comp.* **8**, 2078 (2012).